

Catalysis Science & Technology

www.rsc.org/catalysis



ISSN 2044-4753



PAPER
Bert F. Sels *et al.*
Immobilized Grubbs catalysts on mesoporous silica materials: insight into support characteristics and their impact on catalytic activity and product selectivity

175 YEARS

CrossMark
click for updatesCite this: *Catal. Sci. Technol.*, 2016,
6, 2580

Immobilized Grubbs catalysts on mesoporous silica materials: insight into support characteristics and their impact on catalytic activity and product selectivity†

Annelies Dewaele, Boris Van Berlo, Jan Dijkmans, Pierre A. Jacobs and Bert F. Sels*

Silica materials show a high ability to physisorb the 2nd generation Hoveyda–Grubbs catalyst (HG2) in organic solvents. The interaction with the complex, likely proceeding through hydrogen bonding, is particularly strong with surfaces rich in silanols, wherein geminal silanols show the highest affinity, and therefore mesoporous silicas are the supports of choice. As long as the silica material is sufficiently pure and free of cages, in which high HG2 concentrations can accumulate, the immobilization of HG2 occurs in a very stable manner. Despite the complex stability, exploration of HG2-loaded mesoporous silica supports in metathesis of *cis*-cyclooctene indicated significant diffusional and confinement effects, and therefore control of pore size, pore architecture and morphology in balance with the intrinsic catalytic activity is essential for catalyst design. As metathesis of *cis*-cyclooctene apparently proceeds through the initial formation of linear polymers, followed by backbiting forming cyclic oligomers, potential interference of mass transport and space restriction issues is not surprising. This study shows that the catalyst requirements are best met with the TUD-1 silica support (1.24 wt% HG2). Under such conditions, the heterogeneous catalyst performs as good as the homogeneous one, presenting a thermodynamic distribution of cyclic oligomers. The latter catalyst also showed high catalyst stability in a continuous fixed bed reactor, corresponding to a catalytic turnover number of 18 000. The catalytic rates and catalyst stability are lower when operating in a diffusional regime, therefore long reaction times are required to reach the thermodynamic product distribution. Water removal from the catalyst is also important, not because of HG2 stability reasons, but of lower reaction rates which were measured for hydrated samples, likely due to inhibition of *cis*-cyclooctene uptake in the pores. Mild removal of physisorbed water before immobilization is therefore advised, for instance by thermal treatments, but care has to be taken to keep the silanol density high for firm HG2 immobilization and also to avoid formation of reactive siloxanes, which chemically react with and destroy HG2. Surprisingly, reactive siloxane formation conditions strongly depend on the silica type, with TUD-1 being fairly sensitive to their formation. Finally, the best HG2-loaded TUD-1 catalyst is used successfully in a broad set of other metathesis reactions.

Received 4th November 2015,
Accepted 3rd December 2015

DOI: 10.1039/c5cy01897h

www.rsc.org/catalysis

Introduction

Olefin metathesis exchanges alkyl substituents between olefins and is considered as a very important reaction for a wide range of applications in organic chemistry.^{1–3} This reaction also provides nice opportunities to produce unsaturated and

therefore modifiable polymers.⁴ Well-defined commercially available Grubbs complexes are established as one of the most promising catalysts; they exhibit high catalytic activity under ambient conditions and show great tolerance towards functional groups, air and moisture.^{5,6} Despite industrial demonstrations,⁷ their use has not been fully exploited due to high cost and environmental reasons. The latter issue is typically symbolized by difficult catalyst recovery, leading to Ru contamination of the product. This is disastrous to the production of fine chemicals like pharmaceuticals,^{8–10} but it also implies a loss of precious metal.

Catalyst immobilization on a solid support offers an attractive solution to Ru recovery. The catalyst is not only more practical to separate from the product mixture, but

Center for Surface Chemistry and Catalysis, KU Leuven, Celestijnenlaan 200F, 3001 Leuven, Belgium. E-mail: bert.sels@biw.kuleuven.be

† Electronic supplementary information (ESI) available: Stirring experiments of HG2/MCM-41, correlation plots of ordered mesoporous silica, conversion plots of thermally treated TUD-1 and MCM-41 are provided. (Near)-infrared spectra and nitrogen physisorption measurements of thermally treated TUD-1 and MCM-41, information about ring–chain equilibria and additional ring selectivity experiments are given. See DOI: 10.1039/c5cy01897h

immobilization also allows protection against catalyst deactivation, caused by reported bimolecular decomposition pathways,^{11–13} and may even exert beneficial confinement effects on the conversion rate and product selectivity. The first heterogeneous metathesis catalysts were based on metal oxides or organometallic complexes on silica/alumina. Pioneer work on surface organometallic chemistry was delivered by Basset and Copéret *et al.*,^{14,15} who characterized the active sites using NMR spectroscopy.^{16–18} Several classical strategies have been developed to anchor Grubbs-like complexes to the surface through covalent linkage *via* (a) halide ligands,^{19–25} (b) phosphine ligands or N-heterocyclic carbenes (NHC)^{11,26–36} and (c) alkylidene ligands,^{37–50} or through encapsulation in cage-like pore structures followed by post-reduction of the window size through silylation.^{51,52} Recent publications with regard to these strategies are summarized in excellent reviews.^{53–57} Whereas these immobilization approaches often require sophisticated and laborious synthesis, with alterations of both the support and catalytic complex, an elegant and more practical immobilization strategy for Hoveyda–Grubbs (HG) complexes on silica supports was reported by Van Berlo *et al.*⁵⁸ This novel immobilization strategy is based on a subtle physical interaction between the 2nd generation Hoveyda–Grubbs (HG2) complex and the silica surface. Their synthesis avoids complicated modifications of either catalyst partner, therefore making it industrially very attractive. Though the soft adsorption concept has been studied briefly and its application was expanded successfully by others to new ordered mesoporous silica (OMS) materials like MCM-41 and SBA-15, there is no real consensus on the requirements of the support material of choice.^{59–65}

Next to the high activity of the physically sorbed complexes, shifts in product selectivity between polymerization (ROMP) and ring-opening ring-closing metathesis (RO-RCM) were reported, especially in metathesis of cyclooctene.^{59,60,66} The products of RO-RCM of cyclooctene, *viz.* macrocyclic structures, exhibit unique properties compared to their linear counterparts due to the lack of chain ends,^{67,68} making them potential intermediates as lubricants or plasticizers,^{69,70} and also in the fragrance industry.⁷¹

Despite the recent evaluation of different porous silica materials, no fundamental has been delivered since, to unambiguously clarify the textural and structural requirements of the mesoporous silica to perform fast and stable metathesis. In search for the ideal catalyst support for RO-RCM of *cis*-cyclooctene to macrocycles, we undertook a systematic study to understand better the impact of the support properties (*e.g.* pore size, pore morphology) on the catalytic activity and product selectivity of supported HG2, as well as to assess surface properties that could substantially affect surface adsorption affinity and catalyst stability such as catalyst surface loading, silanol density and type. Furthermore, we addressed typical heterogeneous catalysis aspects like stability in a continuous reaction and discussed mass transfer limitations, rather uncommon in metathesis studies, but necessary to understand heterogeneous metathesis catalysis. Based on these

insights, an optimal support–catalyst system is designed and further used to unravel the reaction pathways of RO-RCM of *cis*-cyclooctene to cyclic oligomers under heterogeneous catalysis conditions. The kinetic study clearly shows kinetic dissimilarities between homo- and heterogeneous reactions due to pore-related issues, all of these being dependent on the type of support and the active site density. Finally, other metathesis types, for which no oligomers and polymers are formed, are also illustrated with the best supported HG2 catalyst.

Results and discussion

Screening of micro- and mesoporous silica

Various potential silica supports such as silica gels, zeolites and OMS were explored to support HG2. The immobilized catalysts were compared for their activity in metathesis of *cis*-cyclooctene, as this substrate is generally used to study the catalytic activity of porous catalysts.^{26,59,60,62,64,72} Moreover, it is an interesting probe to investigate the impact of textural properties on selectivity, as both cyclic and linear oligomers/polymers are formed. Table 1 compares the catalytic performance along with the materials' characteristics. The activity is defined by the initial turnover frequency (TOF_i), *i.e.* the number of moles of cyclooctene converted per mol of Ru per second, in the initial phase of the reaction.

Three zeolites were tested: silicalite-1, AlPO₄-5 and Si-VPI-5 (Table 1, entries 2–4). The pores of silicalite-1 and AlPO₄-5 are obviously too small for adsorption of HG2 (1.18 × 1.07 nm) and therefore contain a very small amount of Ru. Si-VPI-5 has larger pores (1.1 nm) and does adsorb HG2, but the density of hydroxyl groups on its surface, affording anchor points for the complex,⁵⁸ is very low resulting in low Ru loading. None of the zeolites showed true heterogeneous activity. The few complexes present on the material leached into the solution, as was proven by a split-test. In such a test, after 15 minutes of reaction, a portion of the reaction suspension was removed and separated by filtration and transferred into a new vial. The reaction progress of the filtered sample was compared to that of the remaining reaction mixture at different time intervals. The result for HG2/Si-VPI-5, given in Fig. 1A, shows a catalytic contribution owing to soluble HG2.

In contrast, the porous amorphous silica materials like silica gels and OMS are truly heterogeneous, confirming the essential role of surface silanols to firmly anchor HG2. The split-test of HG2/TUD-1 is illustrated in Fig. 1B. Clearly, no activity is measured in the filtrate. Besides showing stable heterogeneous catalysis, the silica gels (Table 1, entries 5 and 6) are reasonably active, with TOF_is ranging between 4 × 10⁻² s⁻¹ and 4.5 × 10⁻² s⁻¹. The lower values, compared to those of some OMS, may be due to the presence of impurities like Na (up to 0.06%) and Ca (0.1%), which modify the surface properties, leading to deactivation of HG2, as suggested in the literature.⁷³

The current wealth of existing OMS should allow a deeper analysis of the relationship between structural and surface

Table 1 Characterization of the supports and activity of the immobilized catalysts

Entry	Material	Ru (wt%)	Split test ^e	D_{particle}^f (μm)	D_{meso}^g (nm)	Morphology	Pore architecture	V_{meso} ($\text{cm}^3 \text{g}^{-1}$)	V_{micro} ($\text{cm}^3 \text{g}^{-1}$)	BET ($\text{m}^2 \text{g}^{-1}$)	TOF_i^h ($\times 10^{-2} \text{s}^{-1}$)
1	HG2 ^c	—	—	—	—	—	—	—	—	—	13
2	Silicalite-1	0.008	—	—	0.54	Coffin	MFI topology	—	—	350	—
3	AlPO ₄ -5	0.001	—	—	0.73	n.d.	AFI topology	—	—	—	—
4	Si-VPI-5	0.12	—	—	1.1	Needles	VFI topology	—	—	—	—
5	Silica gel ^a	0.35	+	2000	n.d.	Irregular	Non-ordered	n.d.	n.d.	375	4
6	Silica gel ^b	0.30	+	50	6	Irregular	Non-ordered	0.72	0	406	4.5
7	KIT-5	0.35	+	10–25	7 ^d	Irregular	Cubic <i>Fm3m</i>	0.30	0.37	1054	1.5
8	SBA-16	0.16	+	4–25	5.5 ^d	Irregular	Cubic <i>Im3m</i>	0.14	0.17	535	2
9	SBA-15	0.29	+	2–5	10	Fibre-like	Hexagonal <i>p6mm</i>	0.98	0.12	791	3
10	SBA-3	0.28	+	1–5	1.8	Platelets	Hexagonal <i>p6mm</i>	0.68	0	1476	3
11	KIT-6	0.26	+	2–5	6	Irregular	Cubic <i>Ia3d</i>	0.72	0.13	700	5
12	MCM-48	0.26	+	0.3–0.7	2.5	Sphere	Cubic <i>Ia3d</i>	0.72	0	1600	5.5
13	SBA-15	0.34	+	0.5–1	5.5	Rope-like	Hexagonal <i>p6mm</i>	0.51	0.51	1097	8
14	C12-MCM-41	0.24	+	0.3–0.5	2.6	Sphere	Hexagonal <i>p6mm</i>	0.34	0	690	8.5
15	C16-MCM-41	0.29	+	0.3–0.5	3.3	Sphere	Hexagonal <i>p6mm</i>	0.67	0	1333	8.5
16	C18-MCM-41	0.33	+	0.3–0.5	3.6	Sphere	Hexagonal <i>p6mm</i>	0.85	0	1446	7.5
17	TUD-1	0.21	+	5–20	8–15	Irregular	Disordered	1.1	0.04	417	10

^a Grace silica gel 239 pellets. ^b Silica gel 60 (Davisil grade). ^c 0.33 mol% HG2 compared to *cis*-cyclooctene. ^d Pore entrance diameter (cage diameter not experimentally determined: KIT-5 (ref. 77) = 6.8–8.3 nm and SBA-16 (ref. 82) = 5.1–7.2 nm). ^e – Split: homogeneous activity; + split: heterogeneous activity. Reaction conditions: 0.05 M *cis*-cyclooctene; 5 mL hexane; 50 mg HG2/support (pretreated at 150 °C); 35 °C. The homogeneous reaction (entry 1) is performed in toluene instead of hexane for solubility reasons. ^f D_{particle} = particle diameter. ^g D_{meso} = mesopore diameter. ^h Error in TOF_i determination is $< 0.5 \times 10^{-2} \text{s}^{-1}$.

characteristics and the catalytic performance (Table 1, entries 7–17). However, our experience reveals a blurred analysis due to a multi-variance of parameters, and therefore drawing general conclusions on activity dependence of *e.g.* particle size (d_{particle}) (Fig. S1†) and pore size (Fig. S2†), based on the whole data set, is not always straightforward. To verify therefore the effect of pore size, three hexagonally pore-ordered mesoporous silicates (MCM-41) having pore diameters of 2.6, 3.3 and 3.6 nm⁷⁴ were tested (Table 1, entries 14–16). Comparable TOF_i s from 7.5 to $8.5 \times 10^{-2} \text{s}^{-1}$ were shown, whereas SBA-3 (Table 1, entry 10), a mesoporous silica with similar pore architecture to MCM-41 as well as similar pore volumes and BET surface area, but a smaller pore diameter of 1.8 nm, showed a lower activity ($\text{TOF}_i = 3 \times 10^{-2} \text{s}^{-1}$). Mass transfer issues, depending on HG2 loading, seem to play a role in cyclooctene metathesis and impact the observed rate and selectivity. Though this point will be addressed later, it is fair to conclude at this stage that 2.5 nm pores (or larger) are

recommended to efficiently catalyze *cis*-cyclooctene metathesis in the presence of 0.2–0.4 wt% Ru-loaded catalysts.

Besides pore diameter, morphology also plays a key role. To prove this, SBA-15 was synthesized in two different morphologies with comparable particle and pore sizes, and loaded with equal contents of HG2: rope-like (Table 1, entry 13) and fibre-like (Table 1, entry 9). Rope-like structures are typical for SBA-15 and have straight channels, whereas fibre-like structures have curving or orbicular channel structures. Though being instrumental in holding the catalyst in the pores, corrugated pores are unfavourable for molecular pore diffusion.⁷⁵ As rope-like SBA-15 performs 2.5 times better than fibre-like SBA-15, intraparticle diffusion is a critical parameter. Additionally, as a large part of the pore volume of rope-like SBA-15 is occupied by micropores (inside the pore walls), not every catalytic complex might be accessible, which then could lead to a lower TOF_i .

Notably, HG2/KIT-5 and HG2/SBA-16 (Table 1, entries 7 and 8) gave the lowest activity of the OMS (TOF_i of 1.5 and $2 \times 10^{-2} \text{s}^{-1}$, respectively), despite their high surface area and large pore size. These two silicas have 3D pore structures with a pronounced cage-like pore system. As the large cages of 5–8 nm allow the formation of large oligomers/polymers of *cis*-cyclooctene, rate retardation is likely a result of internal pore entrance blockage. In addition, we also noticed that HG2 deactivates rapidly within the cage-like KIT-5 and SBA-16 silica, as visually seen by the fast green-to-brown colour change. As the colour variation occurs also in the absence of a substrate, deactivation is likely caused by the fast disproportionation of HG2 due to its high concentration and dynamics in the large cages.⁷⁶ Assuming that HG2 is preferentially located inside the cages and its volume covers a minor

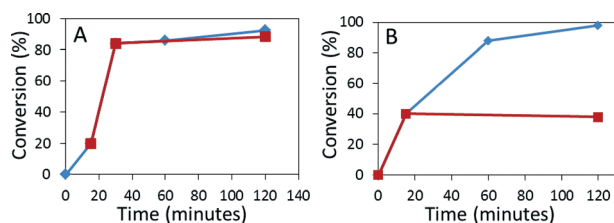


Fig. 1 Two examples of a split-test with Ru leaching for (A) HG2/Si-VPI-5 and without Ru leaching for (B) HG2/TUD-1. Blue curve: liquid phase with the heterogeneous catalyst; red curve: liquid phase after filtration. Reaction conditions: 0.05 M *cis*-cyclooctene; 5 mL hexane; 50 mg HG2/Si-VPI-5 (pre-treated at 50 °C, 0.12 wt% Ru) or HG2/TUD-1 (pre-treated at 150 °C; 0.21 wt% Ru); 35 °C.

part of the total volume (11%),⁷⁷ the volumetric concentration in the pores of KIT-5 can be 35 times higher compared to that of fibre-like SBA-15 (1000 mol_{Ru} m⁻³ vs. 29 mol_{Ru} m⁻³). HG2 is more evenly spread in fibre-like SBA-15, indicating that the low activity of this catalyst is likely caused by low diffusion through the corrugated pore system.

KIT-6 and MCM-48 (Table 1, entries 11 and 12), cubic *Ia3d* structures with a 3D channel network, have similar TOF_s of 5 and 5.5 × 10⁻² s⁻¹, respectively, which are lower than those for one-dimensional hexagonal structures like MCM-41 and SBA-15. Despite their 3D pore network, pore diffusion might be slower due to a higher tortuosity (τ). For instance, linear hexagonal structures like MCM-41 and SBA-15 (Table 1, entry 13) have τ close to 1, whereas $\tau = 3$ for MCM-48.⁷⁸

TUD-1, a highly porous structure with interconnecting cage-free mesopores, attains a high activity close to those of SBA-15 and MCM-41 (Table 1, entry 17). Just like KIT-6 and MCM-48, it has a three-dimensional pore network, although a higher activity is observed. This could likely be attributed to the high porosity and pore structure of TUD-1, providing optimal features for fast intracrystalline diffusion. Awaiting for a profound structural analysis of TUD-1, other factors cannot be excluded. Nevertheless, TUD-1 has often been acknowledged in the literature for its superior catalytic activity, outperforming other ordered mesoporous silicas.^{79–81}

To conclude, metathesis of *cis*-cyclooctene with low loadings of HG2 on mesoporous silica is truly heterogeneous, but care has to be taken to balance diffusion and the internal catalytic activity in order to perform catalysis in the kinetic regime and thus to use the costly HG2 catalyst most efficiently. Pure siliceous mesoporous silicas are recommended, preferably with pores larger than 2.5 nm, the absence of cage-like or bimodal pore systems, and a short diffusion path, which are related to morphology and pore architecture. Rope-like SBA-15, spherical MCM-41 and TUD-1 are the support candidates of choice for *cis*-cyclooctene metathesis because of the absence of diffusion limitations. Their catalytic activity approaches that of the homogeneous complex (Table 1, entry 1).

Influence of solvent polarity on surface mobility and HG2 leaching

For all porous amorphous silicas, irrespective of the particle size, pore size and pore ordering, HG2 remains grafted on the silica surface, as demonstrated above in the catalyst split-tests. To further confirm the true heterogeneity of the catalyst, an additional test was developed to examine the mobility of the complex under reaction conditions. The experiment is illustrated and described in Fig. 2 for silica gel, but the conclusion holds for the other mesoporous silicas.

Ten green pellets of HG2/silica gel were placed in a glass vial and one unloaded white pellet of silica gel was added. Three identical sets of such eleven pellets were brought into contact with a 5 ml toluene solution (A), a substrate mixture of 0.05 M *cis*-cyclooctene in hexane (B), and a mixture of 0.8 M *cis*-cyclooctene in hexane (C). After 4 hours of shaking and

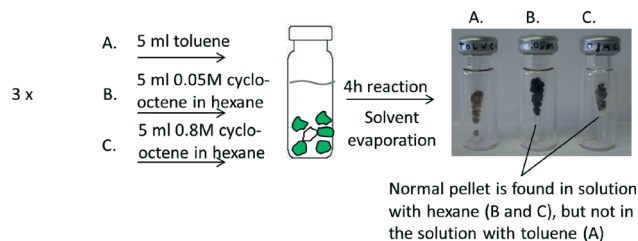


Fig. 2 Mobility experiment to prove the firm anchorage of HG2 on the silica support under varying solvent and substrate concentrations.

solvent evaporation, vial A contained 11 coloured pellets, whereas vials B and C contained one unloaded white pellet next to ten green pellets. In other words, HG2 leaches from the silica support in toluene and is redistributed among the eleven pellets. Under apolar conditions (hexane) and independent of substrate concentration, HG2 remains anchored on the support as no migration was observed throughout the liquid reaction mixture. Physisorption of HG2 on silica is thus truly heterogeneous, provided that the solvent is apolar with restricted solubility of HG2.

Stability of the immobilized catalyst – a continuous experiment

The experiment in Fig. 2 already showed the firm anchoring of HG2 on a silica support under the reaction circumstances, but a continuous experiment is a better measure of catalyst robustness. For the actual experiment, 110 mg of 0.20 wt% Ru-loaded HG2/TUD-1 (pellets) were packed in a reactor together with quartz wool and glass beads. The catalyst bed had dimensions of 0.94 × 3.5 cm. A solution of 0.4 mol L⁻¹ *cis*-cyclooctene in hexane was pumped through the reactor at room temperature dosed at 38 mL g_{cat}⁻¹ h⁻¹. The reactor outlet was sampled at regular times. The accumulated turnover number (TON) is presented in Fig. 3.

Initially, about 40% cyclooctene is converted, but the conversion decreases to 25% after 200 min and faded to 3% at the end of the reaction after 540 min. At this point, a TON of 18000 was obtained, corresponding to a conversion of 39 grams of cyclooctene per gram of catalyst. To the best of our knowledge, this is the highest reported TON for the ROMP of non-purified *cis*-cyclooctene under ambient conditions with an immobilized HG2 complex.

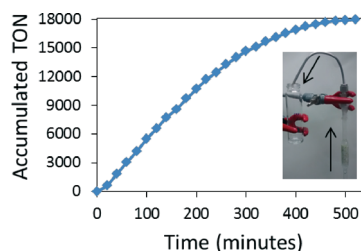


Fig. 3 Accumulated TON in a continuous experiment of HG2/TUD-1. Inset to the right: the set-up of the reaction with the direction of the feed flow.

Thermal treatment of the support

Surface hydroxyl groups were reported to be essential for anchoring HG2, but this was not investigated.⁵⁸ Thermal treatment of silica materials removes physisorbed water molecules from the surface and changes the chemical composition by a surface dehydroxylation process forming siloxane moieties.⁸³ If surface hydroxyls are important in HG2 immobilization, thermal treatment of the parent support material should have a substantial influence on catalyst immobilization. Therefore, prior to HG2 immobilization, MCM-41 (3.3 nm pores) and TUD-1 were subjected to elevated temperature treatments ranging from 150 °C to 900 °C. Samples without treatment, kept at 25 °C, were used as a reference. The immobilization process was conducted under conditions identical to those applied before. The initial activities of variously pre-treated HG2/TUD-1 and HG2/MCM-41, measured as TOF_i, in metathesis of *cis*-cyclooctene are compared in Fig. 4. The corresponding kinetic profiles, obtained by plotting conversion with time, are shown in the ESI† (Fig. S3 and S4). Thermal treatment of MCM-41 leads to a higher activity, the TOF_i increasing with elevating temperature. The activity gain is most pronounced after heating at 150 °C, while a further gradual increase is observed up to 700 °C. Overall, the TOF_i increases from $2.5 \times 10^{-2} \text{ s}^{-1}$ for the untreated MCM-41 up to $10.5 \times 10^{-2} \text{ s}^{-1}$ for the MCM-41 treated at 700 °C. Treatment at 900 °C also leads to an active catalyst, however considerable Ru leaching into solution is observed with this catalyst. The same trend is observed for TUD-1, though the preferred treatment here is below 400 °C. Higher treatment temperatures for TUD-1 lead to inferior catalytic results, accompanied by a fast green-to-brown coloration of the catalyst. A spectroscopic study was performed to rationalize these thermal treatment effects.

The temperature-induced dehydration and dehydroxylation of the silica surface were therefore monitored by (near)-infrared (IR) spectroscopy through changes in the $\nu_{\text{O-H}}$ vibration ($3800\text{--}3000 \text{ cm}^{-1}$) and $(\nu + \delta)_{\text{O-H}}$ ($4800\text{--}4200 \text{ cm}^{-1}$)

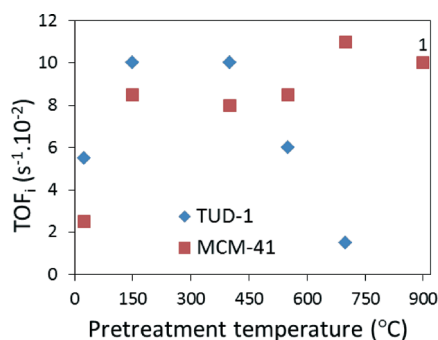


Fig. 4 Influence of thermal treatment of the support on the TOF_i of HG2/TUD-1 (0.21 wt% Ru) and HG2/MCM-41 (0.30 wt% Ru). MCM-41 treated at 900 °C (1) shows considerable leaching, therefore overestimating the contribution of heterogeneous TOF. Reaction conditions: 0.05 M *cis*-cyclooctene; 5 mL hexane; 50 mg HG2/support; 35 °C.

overtone domain at different temperatures. The data of the IR spectroscopic study are collected in Fig. S5.†

Quantification of the silanol density was accomplished by integrating the $(\nu + \delta)_{\text{O-H}}$ absorption bands, as the molar integrated absorption coefficient of these bands $\epsilon_{(\nu+\delta)_{\text{O-H}}}$ does not vary with the nature and concentration of the silanol groups.⁸⁴ At room temperature, the surface is completely hydroxylated, together with a monolayer of physically adsorbed water, while drying the support at 150 °C and atmospheric pressure (or 50 °C under vacuum) removes the hydrogen-bonded water and leaves the hydroxyl groups intact. At higher temperature treatments, geminal and vicinal silanols gradually disappear in favour of isolated silanols and surface siloxanes.⁸³ The silanol densities per gram of TUD-1 and MCM-41 together with the ratio of silanol density per surface area of the two catalysts, *i.e.* TUD-1 to MCM-41, are presented in Table 2.

The silanol density per surface area of the parent material is comparable for the two silica materials and corresponds to 2 OH per square nm, which is in accordance with the literature.⁸³ As expected, the silanol density remains intact after heating until 150 °C, but decreases with elevating temperature, albeit differently for both silicas. Considering the potential anchoring role of silanols, a plot of the total silanol density per Ru site against the initial activity of HG2/TUD-1 and HG2/MCM-41 is constructed in Fig. 5. Untreated materials TUD-1 (25 °C; with 63 OH per Ru) and MCM-41 (25 °C; with 145 OH per Ru) are represented by the blue dots and contain physisorbed water. Dehydration of these materials at 50 °C under vacuum (at 10 mbar) or at 150 °C (at atmospheric pressure) removes this water, but retains the chemisorbed silanols. The chemical equivalence of these two treatments was confirmed by NIR diffuse reflectance spectroscopy (Fig. S6†).⁸⁵ As this dehydration step led to the sharpest increase in activity, as visualized by the blue arrows in Fig. 5, not only is the presence of water clearly disadvantageous for metathesis catalysis, but it can also be concluded that the type of silanol is less crucial for the catalytic activity. As the observation of the typically green colour indicates a stable HG2 on the untreated supports, their lower activity is not caused by catalyst deactivation, but rather polarity effects, retarding *cis*-cyclooctene diffusion in pores filled with water, is the cause of the slow catalysis. In fact, it may be estimated by TGA and surface area measurements that water covers about 20% and 60% of the mesopore surface of MCM-41 and TUD-1, respectively.

Experimental verification of the water effect is accomplished by intentionally adding the amount of water, that is, removed by the thermal treatment from 25 °C to 150 °C, to a water-free HG2/MCM-41 catalyst (pre-dried at 150 °C). Addition of water indeed lowered the TOF_i from $8.5 \times 10^{-2} \text{ s}^{-1}$ to $6.0 \times 10^{-2} \text{ s}^{-1}$ in accordance with the above considerations. The red dots in Fig. 5 represent the activities of thermally treated HG2/TUD-1 and HG2/MCM-41. The thermal treatment was varied between 50 °C (10 mbar vacuum) and higher temperatures (atmospheric pressure). From the right to the

Table 2 Silanol densities ($\text{mmol}_{\text{OH}} \text{g}^{-1}$) of TUD-1 and MCM-41 after pretreatment at elevated temperatures

	25 °C ($\text{mmol}_{\text{OH}} \text{g}^{-1}$)	150 °C ($\text{mmol}_{\text{OH}} \text{g}^{-1}$)	400 °C ($\text{mmol}_{\text{OH}} \text{g}^{-1}$)	550 °C ($\text{mmol}_{\text{OH}} \text{g}^{-1}$)	700 °C ($\text{mmol}_{\text{OH}} \text{g}^{-1}$)
TUD-1	1.30	1.27	0.74	0.53	0.48
MCM-41	4.35	4.35	3.22	2.34	1.59
TUD-1 : MCM-41 ^a	0.96	0.93	0.73	0.73	0.96

^a Ratio of OH density of TUD-1 : MCM-41 (calculated in mmol m^{-2}). TUD-1: $417 \text{ m}^2 \text{ g}^{-1}$; MCM-41: $1333 \text{ m}^2 \text{ g}^{-1}$.

left hand-side, the silanol density decreases as a consequence of the dehydroxylation process. Clearly, high activities are observed as soon as water is removed, leaving sufficient content of silanols, *viz.* at least more than 40 OH per Ru. Treating the parent TUD-1 sample at temperatures higher than 400 °C substantially reduces the catalytic activity, whereas treatment of the MCM-41 support at 900 °C leads to the catalytic activity being unchanged, albeit accompanied by considerable complex leaching in the latter case. Neither of the two phenomena originate from temperature-induced collapse of the pore structure, as N_2 physisorption proved an intact structure for TUD-1 treated at 700 °C and the characteristics of MCM-41 mainly remained unchanged up to 900 °C (although some pore shrinkage occurred at 900 °C) (Table S1†), in accordance with literature-reported data for Si-MCM-41 under the same heating conditions.⁸⁶ As the decrease in activity of HG2/TUD-1 treated at 400 °C is accompanied by a rapid green-to-brown colour change, we hypothesized that the presence of strained siloxane bridges causes catalyst deactivation. Such reactive siloxanes have indeed been described as reactive sites on silica surfaces in different reactions,^{87,88} as well as being responsible for the decomposition of Ru complexes due to Ru–O–Si bond formation.⁷⁶ The concentration of such siloxanes typically increases with the increase in pretreatment temperature, but why the observed catalyst deactivation is only prominent for TUD-1 is unclear. As the difference in siloxane reactivity

may explain this phenomenon, the presence and reactivity of siloxanes were monitored.

An easy chemical method to determine the strained siloxanes involves their reaction with NH_3 under continuous flow at elevated temperature to form Si– NH_2 , after passivating the reactive surface hydroxyl groups with dichlorodimethylsilane (DCDMS).^{89–91} Finally, hydrolysis of the unstable Si– NH_2 in water, forming a silanol and ammonia, and measurement of the pH allow a good estimate of the reactive siloxanes. The chemical surface transformations during the procedure were monitored by FT-IR spectroscopy (Fig. 6).

TUD-1, pretreated at 150 °C, shows an intense vibration band at 3745 cm^{-1} ($\nu_{\text{s}}(\text{OH})$) and a broad shoulder at lower wavenumbers due to hydrogen bonding phenomena (Fig. 6A). After treatment with DCDMS, the band at 3745 cm^{-1} completely disappears at the expense of three new features at 2970 , 2901 and 1460 cm^{-1} , corresponding to $\nu_{\text{s}}(\text{CH}_3)$, $\nu_{\text{as}}(\text{CH}_3)$ and $\delta(\text{CH}_3)$, respectively (Fig. 6B).⁹² The reaction of ammonia with siloxanes is evidenced by the characteristic absorption bands at 3536 , 3452 and 1550 cm^{-1} , attributed to $\nu_{\text{as}}(\text{NH}_2)$, $\nu_{\text{s}}(\text{NH}_2)$ and $\delta(\text{NH}_2)$ vibrations, respectively (Fig. 6C).⁹³ Subsequent hydrolysis and pH measurements allow the determination of the reactive siloxane content. The amount of ammonia recovered per gram of catalyst, as a measure of Si– NH_2 , as well as the corresponding number of siloxanes and the average distance of silanols on the surface of TUD-1 and MCM-41, is presented in Table 3. TUD-1, though treated at lower temperature (here: 550 °C), shows a substantial amount of strained siloxanes, whereas their abundance is ten times lower for an MCM-41 sample treated at 900 °C. The high content of reactive siloxanes on TUD-1 may therefore be considered to cause deactivation of HG2. Though the

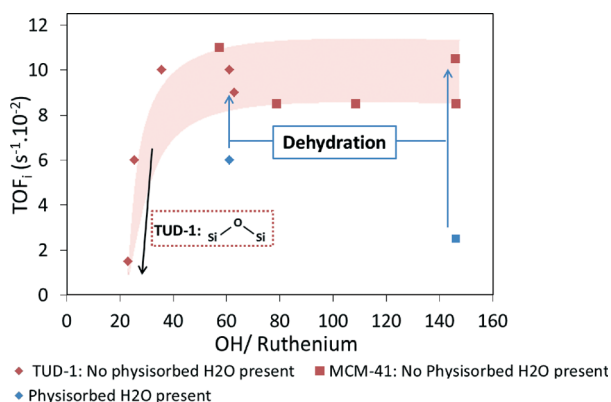


Fig. 5 Influence of the molar ratio of silanols to Ru on the initial activity of the ROMP of *cis*-cyclooctene when physisorbed water is present (blue dots), or with a fully dehydrated support (red dots). Reaction conditions: 0.05 M *cis*-cyclooctene; 5 mL hexane; 50 mg HG2/MCM-41 and TUD-1 (pre-treated at different temperatures; loading of 0.30 wt% Ru for HG2/MCM-41 and 0.21 wt% Ru for HG2/TUD-1); 35 °C.

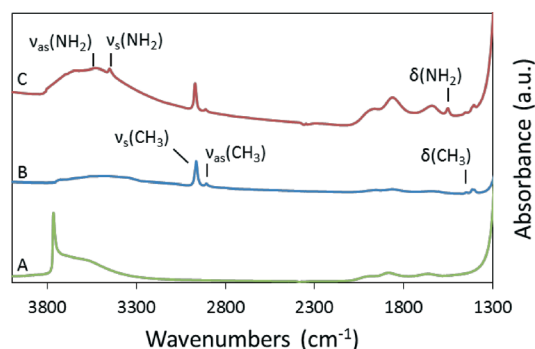


Fig. 6 IR spectra of (A) TUD-1 treated at 150 °C, (B) TUD-1 after passivation with DCDMS and (C) TUD-1 after passivation with DCDMS and reaction with NH_3 .

Table 3 NH₂ contents on TUD-1 and MCM-41

	NH ₃ reacted (mmol g ⁻¹)	Siloxanes ^a (% as OH)	Distance of silanols (nm)
TUD-1 (550 °C)	0.048	3.8	1.3
MCM-41 (900 °C)	0.0037	0.1	2.5

^a Siloxanes reacted with NH₃ divided by total silanol density.

thermally treated MCM-41, being free of siloxanes, keeps HG2 intact in accordance with its green colour, the treatment at 900 °C causes considerable leaching of the Ru complex. The lower affinity to HG2 is likely due to the lesser amount of remaining silanols, isolated at a too large distance from each other (2.5 nm).

In conclusion, for stable metathesis with supported HG2, the mesoporous silica should be treated at elevated temperatures, preferably for MCM-41 and TUD-1 at 50 °C under vacuum (10 mbar) or at 150 °C under atmospheric pressure, prior to immobilization, to remove physisorbed water and to conserve a high amount of silanol anchors for immobilization. Therefore, care has to be taken to prevent the formation of reactive siloxane bridges during thermal treatment of the support so as to keep the surface unreactive toward HG2. Remarkably, the necessity of silanol groups for stabilization of HG2 is in contrast with previous studies that reported the detrimental role of silanol groups in the stability of the 1st generation Grubbs complex.^{50,76,94}

Adsorption isotherms of HG2 on mesoporous silica

As a high affinity of the support for HG2 is desirable to prevent decomposition and leaching, adsorption isotherms of HG2 for MCM-41 (3.3 nm pores) and TUD-1 dried at 150 °C were determined and investigated (Fig. 7). A rise of HG2 concentration in the sorption solution initially results in a linear increase of immobilized HG2 (Fig. 7A), wherein 4 out of 5 HG2 molecules adsorb from the solution on the support, with an adsorption rate of 4 μmol of HG2 per gram per minute. This corresponds to 1 and 3 μmol of HG2 per mmol of

OH per minute for MCM-41 and TUD-1, respectively. At higher concentrations, higher loadings are observed on MCM-41 compared to TUD-1, which is in line with the higher surface area and thus anchoring capacity of MCM-41 per silica weight. A sharp deflection from linear uptake is observed for both TUD-1 and MCM-41 at Ru equilibrium concentrations above 0.7 and 1.7 mM, respectively, indicating that the adsorption process becomes thus less efficient at higher HG2 concentrations. Though pore blockage by HG2 itself cannot be excluded as an explanation for the decreasing uptake efficiency with increasing HG2 loading, the sharp distinctive shape of the isotherms of both materials rather points to the existence of two distinct adsorption sites, one with high affinity (occupied at low loadings) and the other with low affinity for HG2 (at higher catalyst loadings). In the modified adsorption isotherms (Fig. 7B), the uptake profile of HG2 is normalized for the amount of silanols (and at the same time for the surface area as MCM-41 and TUD-1 have equal surface silanol densities of 0.003 mmol m⁻²), rather than for the weight of the catalyst. The deflection of the affinity sets in at 8.2×10^{-5} and 1.2×10^{-4} mmol_{HG2} m⁻² (1.22×10^{-6} and 1.90×10^{-6} mol_{HG2} mmol_{OH}⁻¹ g) for MCM-41 and TUD-1, respectively, corresponding to 1.1 wt% Ru for MCM-41 and 0.5 wt% Ru for TUD-1. The total adsorption capacities at room temperature were estimated to be 3.2×10^{-4} and 1.8×10^{-4} mmol_{HG2} m⁻² for TUD-1 and MCM-41, respectively.

Since both TUD-1 and MCM-41 materials show comparable OH surface densities (Table 2), a difference in the surface uptake behaviour of the respective silicas was not expected. The plot nevertheless reveals a higher affinity of the TUD-1 silica surface and thus thermodynamically more favourable

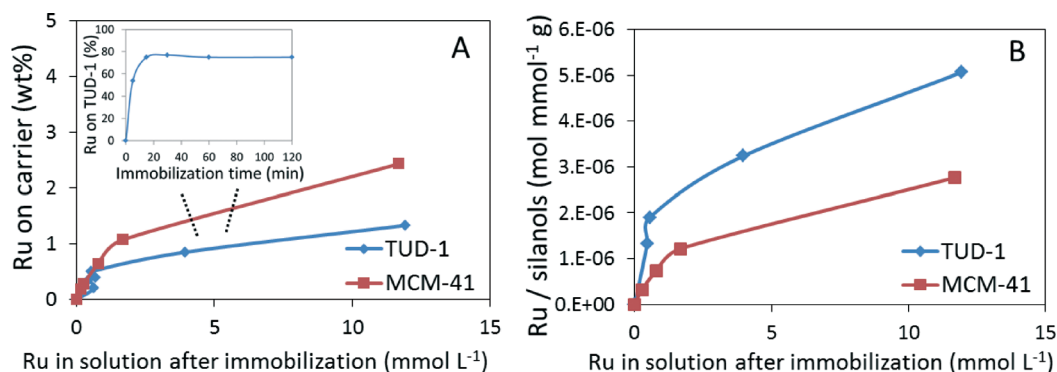


Fig. 7 (A) Carrier loading (wt%) of Ru on TUD-1 and MCM-41 at different concentrations of HG2 in toluene. The kinetic profile of immobilization is presented in the inset. For both materials, the adsorption equilibrium was reached after 30 minutes, and therefore the adsorption isotherm experiments were run for 45 minutes to obtain thermodynamically sound HG2 uptake values. (B) Modified adsorption isotherms of Ru on TUD-1 and MCM-41. Both supports were pre-treated at 150 °C prior to immobilization.

adsorption sites are present when compared to that of MCM-41. ^{29}Si MAS NMR of the surface of both support materials, pretreated at 150 °C, was therefore studied. By distinguishing the signal for isolated and geminal silanols, according to Ide *et al.*,⁹⁵ clear structural differences were observed: TUD-1 treated at 150 °C has a substantially higher fraction of geminal silanols ($Q_2/(Q_3 + Q_2) = 0.19$) compared to similarly dried MCM-41 ($Q_2/(Q_3 + Q_2) = 0.10$), suggesting that HG2 more favourably interacts with that silanol type. The amount of geminal silanols exceeds the linear uptake of HG2 with a factor 5 for TUD-1 and 3.5 for MCM-41, corresponding to a higher density of $5.7 \times 10^{-4} \text{ mmol m}^{-2}$ on TUD-1 compared to $3.1 \times 10^{-4} \text{ mmol m}^{-2}$ on MCM-41. Awaiting for additional arguments for the (enthalpic) difference in surface adsorption chemistry, steric (entropic) factors due to space restrictions, most pronounced in the smaller pores of MCM-41, cannot be excluded.

Influence of active site density on catalytic activity

Heterogeneous metathesis reactions are preferably carried out with highly loaded HG2 complexes, as long as HG2 instability and pore diffusion limitations (PDL) are absent. The optimal active site density was therefore searched for by systematically increasing HG2 loading, ranging from 0.1 to 2.5 wt% Ru, on MCM-41 (3.3 nm pores) and TUD-1 dried at 150 °C. The total catalyst weight in the catalytic tests remained constant (50 mg). All immobilized catalysts were bright green and thus not affected by deactivation. Whereas both supports show increasing conversion rates with higher HG2 loadings (Fig. S7[†]), the activity per catalytic complex (TOF_i), as shown in Fig. 8, indicates a steeper decrease of the TOF_i for HG2/MCM-41. Such behaviour is less obvious for HG2/TUD-1 as only a slight drop of the TOF_i to $9 \times 10^{-2} \text{ s}^{-1}$ is observed at 1 μmol of HG2, corresponding to 2.1 wt% Ru.

Therefore, loadings up to 2 wt% are possible on TUD-1 without losing catalyst efficiency. Indeed, the experimental verification, where the TOF_i is compared between two reactions with catalysts having different catalytic loadings, is called the Koros and Nowak criterion. According to this

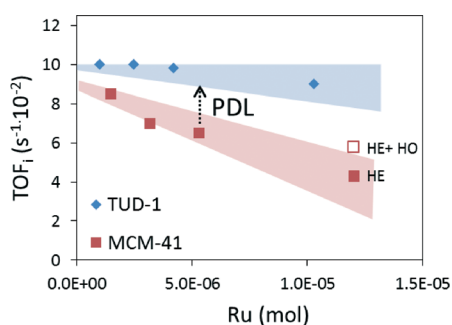


Fig. 8 Influence of the abundance of ruthenium per catalyst volume on the initial activity (TOF_i). PDL = pore diffusion limitations; HE = heterogeneous activity; HO = homogeneous activity. Reaction conditions: 0.05 M *cis*-cyclooctene; 5 mL hexane; 50 mg HG2/TUD-1 or HG2/MCM-41 (pre-treated at 150 °C); 35 °C.

criterion, PDL is excluded whenever the turnover frequency is invariant of the density of the active sites.⁹⁶ This criterion is only valid under the following conditions: (1) isothermal reactions with negligible thermal gradients; (2) every added catalytic complex should be identical to the previous one and represent one catalytic site.⁹⁷ As these conditions are satisfied in our work, the rate of cyclooctene metathesis with HG2/TUD-1 up to 2 wt% Ru is determined by the catalytic reaction and not by mass transport. Higher loadings though will render the catalysis inefficient due to PDL, thus resulting in artificial underestimation of TOFs.

HG2/MCM-41 has a steeper activity decrease from $8.5 \times 10^{-2} \text{ s}^{-1}$ at 1.5 μmol of HG2 (0.30 wt% Ru) to $6 \times 10^{-2} \text{ s}^{-1}$ at 12 μmol of HG2 (2.4 wt% Ru) and seems thus more susceptible to mass transport phenomena than HG2/TUD-1. In fact, this conclusion is in line with the smaller pore size of MCM-41 (3.3 nm) compared to that of TUD-1 (8–15 nm). The decrease in activity could be attributed to a lower effective cyclooctene concentration in the pores leading to a lower activity on one hand, or to a less accessible active Ru site caused by pore obstruction on the other hand. The true mechanism behind this decrease in activity was unravelled by carefully investigating the product selectivity and will be discussed in the next section.

Note that extrapolation of the catalytic activity towards low Ru loading, thus free of PDL, shows fairly similar TOFs irrespective of the mesoporous silica type, the value being close to that of the homogeneous HG2 catalyst. This means that despite dissimilarities in affinity and precise anchoring of HG2, no essential impact on the catalytic activity between the two supported HG2 catalysts is observed.

The original activity of the highly loaded HG2/MCM-41 (2.4 wt% Ru) on the graph in Fig. 8 seems erroneous, as a TOF well below the observed value of $6 \times 10^{-2} \text{ s}^{-1}$ was expected due to PDL contribution. A split test and ICP-AES analysis of the reaction solution pointed to significant leaching of HG2 for this highly loaded MCM-41. Subtracting the homogeneous activity of HG2 gives a true heterogeneous contribution (HE) of $4.3 \times 10^{-2} \text{ s}^{-1}$, which better fits the expectations. Besides confirming mass transfer issues with MCM-41, this experiment shows that stable anchoring of HG2 with high loadings are better accomplished on TUD-1.

Kinetic dissimilarities between supported and non-supported HG2

The enthalpic driving force of cyclic molecules like cyclooctene enables them to undergo irreversible ROMP metathesis, thereby releasing ring-strain. The formation of linear polymers is therefore accompanied by the formation of low-molecular-weight cyclic oligomers, which originates from the direct cyclo-oligomerization of cyclooctene or from polymer backbiting.⁹⁸ The final ring-chain equilibrium is, besides the catalyst and ring-strain of the cycloolefin, mostly dependent on the monomer concentration.^{99,100} In 1950, Jacobson and Stockmayer (J-S) developed a theory of ring-chain equilibria,

including a prediction of the statistical distribution of cyclic structures at equilibrium. While at low monomer concentrations mostly cyclic oligomers are formed, linear polymers are formed at high concentrations. The highest concentration in which no linear polymers were formed at an equilibrium situation was defined as the critical monomer concentration.¹⁰¹ This model was later refined by Kornfield *et al.*, taking into account the ring-strain phenomenon, which was neglected in the J-S theory¹⁰² (for further theoretical background, see the ESI†). The critical concentration $[M]_{c,\infty}$ was hereby calculated to be 0.21 mol L⁻¹ for cyclooctene, in agreement with experimental data. Thus, at concentrations lower than 0.21 M, mostly cyclic oligomers are formed in the presence of homogeneous metathesis catalysts. The successful employment of the homogeneous HG2 complex for the formation of a library of macrocycles was already demonstrated multiple times in the literature.^{103–105}

Driven by our interest in selectively synthesizing cyclic oligomers, we evaluated this reaction at low monomer concentrations with a homogeneous HG2 catalyst and compared the catalytic outcome (product selectivity) with that of a reaction in the presence of the immobilized complex on porous silica under batch conditions. The potential of this reaction was proposed earlier by us¹⁰⁶ and later by research groups centred around BASF,⁶⁶ and described under continuous-flow conditions.⁶⁰ As heterogeneous reactions are often confronted with confinement and diffusion issues, kinetic dissimilarities between homo- and heterogeneous metathesis catalysed reactions may be expected.¹⁰⁷ This will especially be likely when linear oligomeric and polymeric products are involved in heterogeneous ROMP reactions. Careful product analysis was therefore attempted during the metathesis of cyclooctene in the presence of homogeneous HG2 and HG2/MCM-41 (3.3 nm pores; 0.30 wt% Ru). Cyclic oligomers up to the pentamer (C40) were analysed by GC, whereas the larger non-volatile macrocycles (C48–C56) together with linear oligomers and polymers were monitored by GPC to complete the mass balance. The molecular weight range of these fractions is provided in the method section (Catalytic Reactions) and extra information about GPC analysis is reported in the ESI† (Fig. S8).

The experimental results of a homogeneous reaction (0.05 M *cis*-cyclooctene) are presented in Fig. 9. At low cyclooctene

conversion, mostly linear oligomers and small cyclic oligomers are formed with a minor amount of linear polymers. As the reaction proceeds, the linear polymer and oligomer fraction is converted almost exclusively to cyclic oligomers (Fig. 9A). Extrapolation of the initial development of the reaction to zero conversion indicates that linear polymerization largely overrules the initial direct formation of cyclic oligomers from cyclooctene (Fig. 9A and B). The cyclic oligomers are predominantly formed through backbiting of the growing linear oligomer and polymer chains which, once formed, are quickly converted. This kinetic reaction pattern was similar to the ones observed with Grubbs II and Grubbs–Nolan catalysts.¹⁰⁴ The cyclic oligomer fraction maximizes at 46% conversion (selectivity of 98%), and the selectivity decreases only slightly to 94% at full conversion in favour of larger cyclic oligomers (4%) and linear oligomers (2%) upon reaching thermodynamic equilibrium (Fig. 9B). The majority of the cyclic fraction consists of C16–C56 cyclic oligomers and the weight distribution is given in Fig. 9C, which was consistent with equilibrium distributions obtained by different authors.^{60,104,108} The observed equilibrium ring distribution was compared to the one predicted by the original J-S theory, as indicated by the black bullet points in Fig. 9C, which foresees a decrease of the molar cyclic oligomer concentration C_i (with degree of polymerization i) with increasing ring size proportional to $i^{-5/2}$. The equilibrium distribution observed here clearly does not obey this theory, since the dimer C16 is overestimated and its concentration (on weight base) is surpassed by that of the trimer C24, likely due to enthalpic reasons as C16 has a higher ring-strain compared to C24 (which is neglected in the J-S theory).¹⁰² Furthermore, the proportion of larger cyclic oligomers exceeds the predicted values. Based on the experimental data, relative molar equilibrium constants K_i of cyclic oligomers with a degree of polymerization i were determined and compared to those obtained by the J-S theory and the refined model of Kornfield and coworkers (Fig. S9†). For cyclic oligomers larger than the trimer C24, the predicted slope of -2.5 is well approximated; the deviation of K_i from theoretical values is larger for smaller cycles.

The reaction was performed as well at other monomer starting concentrations. At low concentrations, *i.e.* 0.025 and 0.1 M, C16–C56 cyclic oligomers are formed almost

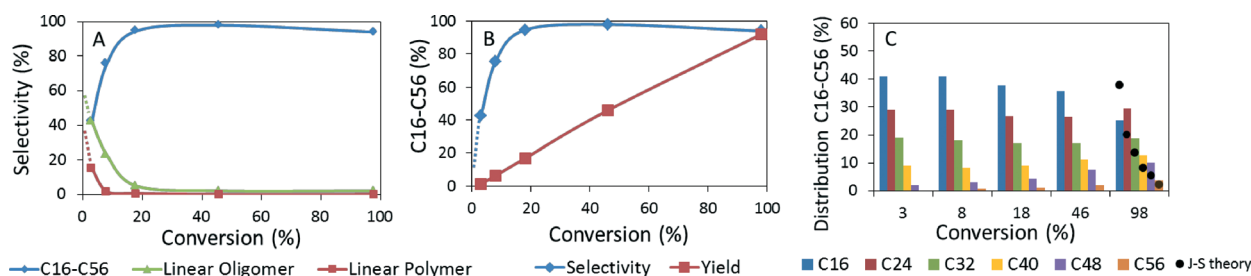


Fig. 9 Homogeneous RO-RCM of *cis*-cyclooctene. (A) Distribution of the cyclic oligomer/linear oligomer/linear polymer fraction as a function of conversion. (B) Yield and selectivity to C16–C56 with increasing conversion. (C) Distribution (wt%) of C16–C56 cyclic oligomers. Reaction conditions: 0.05 M *cis*-cyclooctene; 16 mL toluene; 3 mg HG2; 35 °C.

exclusively at equilibrium, reaching 99 and 91% product selectivity, respectively. At higher concentrations (0.3 M), this fraction drops to 65%, which is reasonable since the initial monomer concentration exceeds the critical concentration of 0.21 M. A graphical representation of this ring-chain equilibrium at different concentrations is shown in Fig. S10.† The distribution within the C16–C56 cyclic oligomer fraction seems also related to this critical concentration. The results are presented in Table 4. At concentrations below $[M]_{c,\infty}$, the ring distributions are identical, while at 0.3 M, larger cyclic oligomers (C40–C56) are more prominent. This is due to the fact that the critical concentration of cyclic oligomers increases proportional to their ring size.¹⁰⁹

At low conversions, the effect of concentration on the product distribution is even more pronounced. While at low monomer starting concentrations, cyclic oligomers are predominantly formed through backbiting of (long) linear chains, as indicated for 0.05 M in Fig. 9A and B, the initial cyclic oligomer concentration decreases at higher concentrations. For instance, at a cyclooctene conversion of 5%, the selectivity towards cyclic oligomers decreases from 54% at 0.025 M to 39% at 0.1 M and 26% at 0.3 M, in favour of (long) linear chains (Fig. S11A†). As polymer growth depends on monomer concentration, in contrast to polymer backbiting, which is the main route to cyclic oligomers under these reaction conditions, it is conceivable that a higher monomer concentration leads to a higher degree of polymerization initially. Moreover, the lower the initial monomer concentration, the higher the probability of direct cyclic oligomer formation. The ratio between the C16–C56 fraction likewise changes with increasing monomer concentration. In particular, the contribution of C40–C56 cyclic oligomers increases (at 5% conversion) (Fig. S11B†). Although the selectivity towards C16–C56 is lower at higher concentrations (0.1 and 0.3 M), its molar concentration is still higher compared to *e.g.* 0.05 M, enhancing the self-metathesis of cyclic oligomers (C16 + 16 = C32 or C16 + C24 = C40), thus affording C40–C56-enriched concentrations.

Impacting the kinetic product distribution is not limited to variation of the feed concentration, as the catalyst itself may also contribute hereto. Kavitake *et al.* showed that with an unsymmetrical NHC-modified catalyst, a 2:1 ratio of C16:C24 could be obtained at low conversions, attributed to the dual-site configuration of the homogeneous catalyst.¹⁰⁴

Table 4 C16–C56 cyclic oligomer distribution at equilibrium starting from different *cis*-cyclooctene concentrations

	C16	C24	C32	C40	C48	C56
0.025 M	25	29	20	14	8	4
0.05 M	25	30	20	14	8	4
0.1 M	23	28	20	14	10	5
0.3 M	18	25	20	17	13	6

Reaction conditions: 0.025–0.3 M *cis*-cyclooctene; 16 mL toluene, 3 mg HG2; 35 °C.

Depending on the steric confinement, the active catalyst selectively discriminates between ring-closing and propagation. After 30% conversion of 0.025 M cyclooctene, C16 and C24 are formed with 57 and 27% selectivity, respectively, while our observed ratio of C16:C24 is much lower (1.5:1) at 20% conversion of 0.025 M cyclooctene with the symmetrical HG2 catalyst.

The homogeneous conversion of the RO-RCM of cyclooctene was compared to that of a heterogeneous reaction with HG2/MCM-41 (0.30 wt% Ru), as displayed in Fig. 10. Initially, linear oligomers and polymers are formed next to a large fraction of C16–C56 cyclic oligomers (Fig. 10A). Compared to the unsupported HG2, a higher initial C16–C56 selectivity was obtained (56% at a conversion of <2%). As the reaction proceeds, the linear polymer fraction reaches a maximum of 25% at 33% conversion and undergoes further backbiting to cyclic oligomers at prolonged reaction times. At full conversion, the reaction mixture comprises 87% of C16–C56 cyclic oligomers and 8% of linear oligomers (mass balance of 95%), while larger cyclic oligomers (>C56) are neglected because of their low abundance. The larger fraction of linear oligomers in the presence of the supported HG2 at an equilibrium situation, *viz.* 8% *vs.* 2%, could be ascribed to secondary intermolecular chain transfer reactions. Hereby, a rearrangement of double bonds occurs between two different nearby growing polymer chains, a phenomenon that seems plausible in the pores of a heterogeneous catalyst where adjacent Ru-polymer chains can interact closely.¹¹⁰ The previous observations though were surprising as the formation of linear polymers was not reported in earlier studies with heterogeneous ROMP of cyclooctene, neither was this observed in that extent in our homogeneous reaction.^{59,60} These results do, however, demonstrate the potential of heterogeneous metathesis in depolymerization reactions of *e.g.* polybutadiene to multiple unsaturated macrocycles. Fig. 10B displays the yield and selectivity to the cyclic fraction as a function of conversion, while the product distribution within the C16–C56 fraction is presented in Fig. 10C. Although the distribution practically equals that of the homogeneous reaction, the contribution of C48 is slightly higher homogeneously. A C40:48 molar ratio of 1.3 was obtained with the soluble HG2, and increased to 1.8 in the presence of the supported HG2.

Most pronounced dissimilarities between the homo- and heterogeneous catalysed reaction, *i.e.* the higher initial C16–C56 cyclic oligomer selectivity and the presence of linear polymers up to 25%, are derived from the peculiar metathesis catalysis occurring in the pores of the catalyst. Diffusion problems of cyclooctene into the pores (*vide supra*, Fig. 8) lead to a lower effective cyclooctene concentration in the pores, stimulating the direct formation of cyclic oligomers instead of linear chains. The C16–C56 fraction reaches therefore a higher initial selectivity of 60% (5% conversion) in comparison with the unsupported HG2. The presence of diffusion problems of cyclooctene into the pores implies that the same is valid for the diffusion of products out of the pores into the bulk. As a result, the formed cyclic oligomers

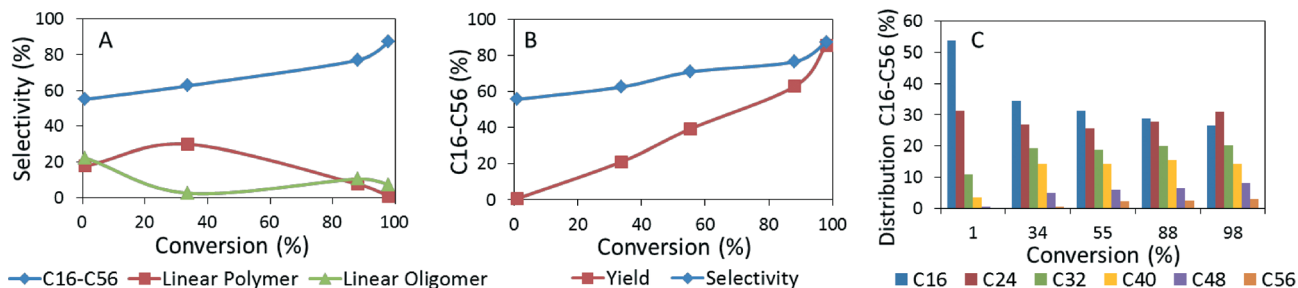


Fig. 10 Reaction profile of heterogeneous RO-RCM of *cis*-cyclooctene with HG2/MCM-41. (A) Distribution of the cyclic oligomer/linear oligomer/linear polymer fraction as a function of conversion. (B) Yield and selectivity to C16–C56 with increasing conversion. (C) Distribution of C16–C56 cyclic oligomers (wt%). Reaction conditions: 0.05 M *cis*-cyclooctene; 16 mL hexane; 160 mg HG2/MCM-41 (pretreated at 150 °C; 0.30 wt% Ru); 35 °C.

tend to react further into linear oligomers and polymers. The indirect formation of cyclic oligomers through backbiting is hindered due to pore confinement effects and the linear chains accumulate in the pores.

Pore diffusion also creates a product shift within the C16–C56 cyclic oligomer fraction. The difficult diffusion of cyclooctene (C8) in and the diffusion of larger cyclic oligomers out of the pores induce a lower C8:C16 ratio inside the pores. As a consequence, C16 cyclic oligomers tend to undergo self-metathesis, forming C32 (schematic representation in Fig. S12†). A higher C32:C24 ratio is thus expected and also observed with the immobilized catalyst, as supported by the data in Fig. 11.

These kinetic differences between homo- and heterogeneous HG2 catalysis disappear at full conversion so as to obey the thermodynamic equilibrium distribution.

The equilibrium situation attained with HG2/MCM-41 was further compared with the homogeneous reaction at different concentrations. Overall, a lower selectivity towards the cyclic C16–C56 fraction is attained at equilibrium with the supported HG2, in favour of linear oligomers, which is clearly visible in Fig. 12 (eq. distribution of cyclic oligomers in Fig. S13†). While at 0.025 and 0.05 M, this linear fraction is rather small, it reaches a value of 20% after reaction with 0.1 M cyclooctene (GPC, inset in Fig. 12) with a corresponding C16–C56 selectivity of 70% (mass balance of 90%). Similar to the

reaction with 0.05 M cyclooctene, kinetic dissimilarities were observed at low cyclooctene conversions of reactions with 0.025 M and 0.1 M cyclooctene. The results are summarized in Table 5. On one hand, the maximal yield of linear polymers increased with concentration, and due to diffusion problems of cyclooctene in the pores, the initial selectivity towards C16–C56 cyclic oligomers increased at 0.1 M. This effect was less pronounced at 0.025 M. Product shifts within the C16–C56 fraction on the other hand were likewise observed at 0.025 and 0.1 M; lower C16:C24 and C24:C32 ratios at a concentration of 0.025 M were apparent, while the contribution of C40 increased at 0.1 M. Kinetic distribution plots (analogous to Fig. 11) are set up for these concentrations in Fig. S14.†

Based on previous results, it can be deduced that the presence of diffusion issues in confined systems may have a significant contribution to the observed product distribution. Either better mass transport in a more open pore architecture, like in TUD-1, or lower Ru loadings should therefore bring the catalytic outcome of the HG2-supported silica system closer to the homogeneous one.

The impact of the Ru loading on the product selectivity was analysed first, since Fig. 8 indicates that the catalytic

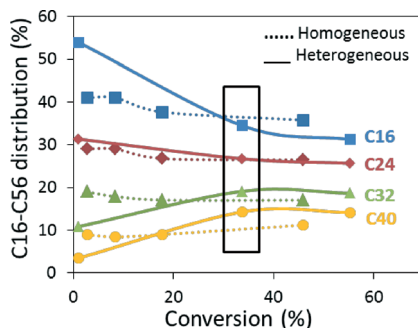


Fig. 11 Distribution of C16–C40 cyclic oligomers for homogeneous and heterogeneous catalysed metathesis of *cis*-cyclooctene (0.05 M). Reaction conditions: see Fig. 9 and 10.

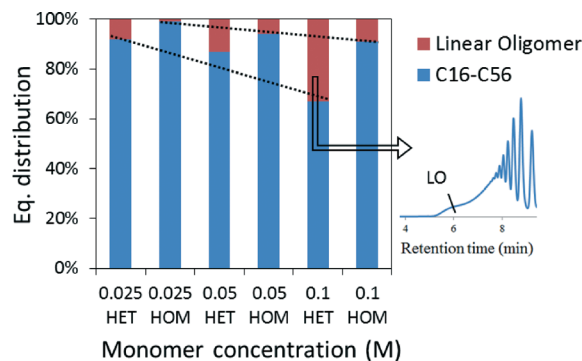


Fig. 12 Equilibrium distribution of homo- and heterogeneous metathesis of *cis*-cyclooctene at different monomer concentrations. Inset: GPC chromatogram of a heterogeneous 0.1 M reaction. LO: linear oligomer; HET: heterogeneous; HOM: homogeneous. Reaction conditions: see Fig. 9 and 10.

Table 5 Selectivity towards C16–C56 cyclic oligomers at 5% conversion at different monomer concentrations

	0.025 M	0.05 M	0.1 M
Homogeneous	55	52	39
Heterogeneous	53	60	45

Reaction conditions: see Fig. 9 and 10.

activity per Ru decreases with increasing Ru density on MCM-41. Reactions were therefore performed with 0.3, 0.6 and 1.2 wt% Ru on MCM-41 and their product distributions were compared. At low cyclooctene concentrations, the contribution of linear polymers augments with higher Ru-loaded catalysts (at 20–30% conversion). As was mentioned above, cyclic oligomers are mainly formed through polymer backbiting in the absence of space restriction. However, inside the pores of MCM-41, polymer accumulation occurs because the backbiting is slow due to pore restrictions, followed by slow diffusion of cyclic oligomers larger than cyclooctene out of the pores, while also reacting to linear polymers. With increasing Ru loading, the probability of cyclic oligomers to react further into linear polymers is therefore enhanced. As a result, pore obstruction makes the active site less accessible for cyclooctene resulting in lower TOF_is (*vide supra*, Fig. 8). At the end of the reaction, significant amounts of carbon residue, expectedly held inside the catalyst pores, were analysed by TGA. The existence of such carbon residue prevents the reaction from reaching a product distribution according to the thermodynamic equilibrium, and this was indeed manifested in the product distribution. At full conversion, the yield of C16–C56 cyclic oligomers only amounts to 71% with 0.6 wt% Ru and 42% with 1.2 wt% Ru; moreover, the perceived distribution within the C16–C56 fraction resembles a kinetic product distribution (Fig. S15[†]). Both phenomena confirm a non-equilibrium state after reaction with highly Ru-loaded MCM-41.

Next, to further examine the relationship between the product distribution and pore restrictions, two other heterogeneous catalysts with more open pore systems were investigated as well, *i.e.* TUD-1 and KIT-5. Recalling the data in Table 1, HG2/KIT-5 has a cage-like pore system and showed a much lower TOF_i compared to HG2/MCM-41, while HG2/TUD-1 has a three-dimensional pore system with 8–15 nm pores and showed a slightly higher TOF_i. The selectivity to C16–C56 cyclic oligomers and linear chains was compared between the three catalysts and the results are presented in Fig. 13. As shown before, TUD-1 with its open structure and containing 0.21 wt% Ru experiences almost no pore diffusion limitation, and indeed the reaction pattern of the cyclic oligomers closely resembles that of the homogeneous reaction (Fig. 9A). The formation of the C16–C56 fraction with HG2/KIT-5, in contrast, bears a resemblance to the pattern of HG2/MCM-41, but only attains a final C16–C56 selectivity of 75%. More surprisingly, almost no linear chains are noticed. Obstruction of polymers in the cages is the most obvious

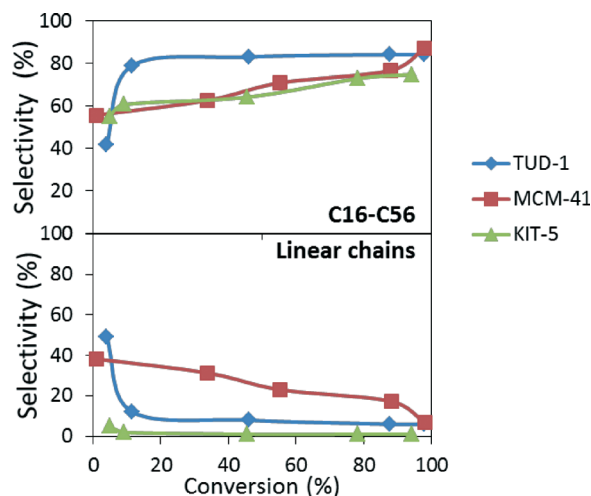


Fig. 13 Selectivity towards the C16–C56 fraction (upper figure) and linear chains (lower figure) with HG2/TUD-1 (0.21 wt% Ru), HG2/MCM-41 (0.30 wt% Ru) and HG2/KIT-5 (0.31 wt% Ru). Reaction conditions: see Fig. 10.

explanation for the diffusion of the polymers out of the silica particles being impeded. Only 75% of the mass was analysed in solution at the end of the reaction, while the deficient part was found on the spent catalyst using TGA analysis.

The main differences between homo- and heterogeneous metathesis of cyclooctene are summarized in the reaction scheme in Fig. 14. Linear polymerization dominates the

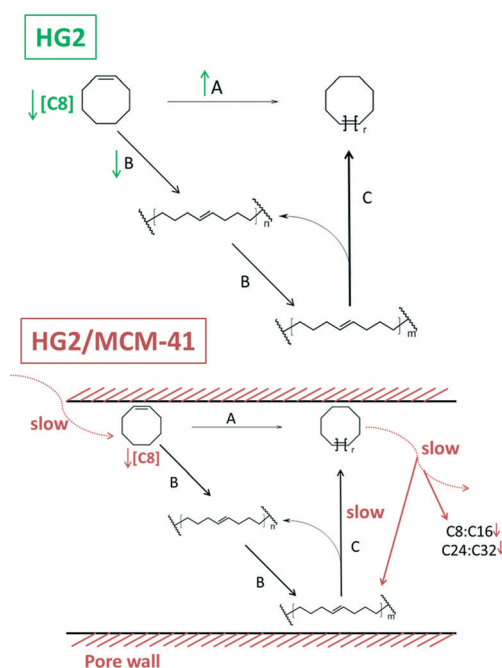


Fig. 14 Proposed reaction scheme for the ring-chain distribution of cyclooctene with HG2 (green) and HG2/MCM-41 (red) under steady-state circumstances. Route A: direct formation of cyclic oligomers from cyclooctene. Route B: polymerization of cyclooctene to linear chains ($n < m$). Route C: backbiting of the polymer chain to cyclic oligomers.

direct formation of cyclic oligomers under homogeneous conditions, causing cyclic oligomers to be formed primarily through backbiting of the linear polymer chains. This effect is most pronounced at high cyclooctene concentration. Heterogeneous reactions with low Ru loadings supported on silica with large pores and an open pore architecture like TUD-1 proceed similarly, and therefore sufficiently high contact times are advised for reactions with these catalysts in continuous fixed-bed plug flow reactors.

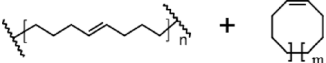
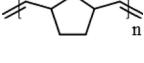
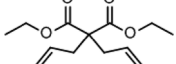
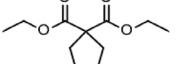
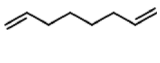
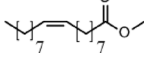
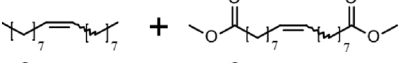
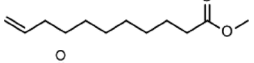
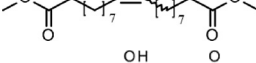
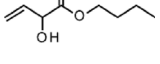
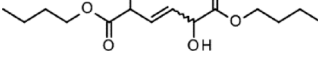
Heterogeneous reactions under the conditions of pore restriction (or high Ru loading), like in the case of HG2/MCM-41, exhibit large differences hereto. They proceed under diffusional control leading to slower reaction rates. Because of the diffusional regime, mixtures of linear and cyclic oligomers are formed, which only turn into comparable cyclic oligomers at full conversion. Yet, the reaction proceeds slower (per Ru) and therefore these catalysts are less interesting for production of cyclic rings from cyclooctene.

Use of HG2/TUD-1 in several metathesis reaction types

Being the best catalyst of choice, HG2/TUD-1 was further exploited in ROMP (Table 6, entries 1–3), ring-closing metathesis (RCM) (Table 6, entries 4 and 5) and cross-metathesis (CM) reactions (Table 6, entries 6–8) of other substrates. For cyclooctadiene (Table 6, entry 2), the initial TOF was lower than that of its mono-unsaturated counterpart (Table 6, entry 1), but cyclic oligomers were selectively produced. The ROMP

of norbornene (Table 6, entry 3) was conducted at a lower concentration of 0.005 M due to its high reactivity as a consequence of the presence of internal bridges. Full conversion was already reached after 15 minutes. The catalyst also showed good activities in the ring-closing metathesis reactions of diethyl diallylmalonate (Table 6, entry 4) and 1,7-octadiene (Table 6, entry 5), as high TOFs were obtained and full conversion was reached after 90 minutes. These two substrates were subjected to additional catalytic tests to evaluate the catalyst robustness in RCM reactions at low catalyst loadings. With 0.5 M diethyl diallylmalonate and 1,7-octadiene, 0.06 mol% HG2/TUD-1 (0.21 wt% Ru) at 35 °C and TONs of 1290 and 1350 were obtained, respectively. Self-metathesis of methyl oleate (Table 6, entry 6) to 9-octadecene-1,18-dioate, a valuable intermediate for the production of polymers and fine chemicals, was also very successful, even at low catalyst concentration. Cross-metathesis of methyl 10-undecenoate was accomplished at 50 °C, yet 2.5 mol% Ru was needed to reach full conversion (Table 6, entry 7). CM of terminal olefins is known to be more challenging, as it lacks the ring-strain release of ROMP and the entropic driving force of RCM.¹¹¹ Finally, the cross-metathesis of butyl vinyl glycolate (Table 6, entry 8) was conducted. This novel renewable substrate can be derived in the methyl ester form from glycolaldehyde and tetroses.^{4,130,131} Transesterification with *n*-butanol makes this compound more soluble in hexane. The dimeric product, which is formed in high yields at 50 °C with 1.2 mol% ruthenium, can be a valuable intermediate in the production of new bio-based polymers.⁴

Table 6 Various metathesis reactions (ROMP, RCM and CM) performed with HG2/TUD-1^a

Entry	Substrate	Product	Time [min] (<i>T</i> [°C])	Conv. [%] [TOF (h ⁻¹)]	Conv. split 15 min [%]	Conv. split end [%]
1			90 (35)	96 [360]	40	40
2			90 (35)	99 [126]	13	12
3 ^b			15 (35)	99 [342]	57 ^f	58
4			90 (35)	99 [306]	32	33
5			90 (35)	98 [468]	52	52
6 ^e			180 (35)	83 [470]	51	51
7 ^c			90 (50)	98 [138]	86 ^g	86
8 ^{d,e}			90 (60)	90 [330]	87 ^g	88

^a 0.05 M substrate; internal standard *n*-undecane; 5 mL hexane; 0.4 mol% Ru; 35 °C. ^b 0.005 M substrate. ^c 2.5 mol% Ru. ^d 1.2 mol% Ru. ^e Reactions were performed in nonane under reduced pressure (700 mbar) to efficiently remove ethylene. ^f Split test after 5 min. ^g Split test after 10 min.

Conclusion

The 2nd generation Hoveyda–Grubbs (HG2) catalyst was immobilized on a series of porous silica materials and tested in the metathesis of *cis*-cyclooctene. High densities of silanols are required to firmly anchor HG2, with the geminal types showing the highest affinity. The affinity of the silica surface for HG2 reduces with HG2 loading. Loadings above 2 wt% should therefore be avoided as they cause HG2 leaching. Cages in the silica pore structure should also be avoided as they result in HG2 degeneration.

The metathesis reaction proceeds under the chemical regime, and is therefore efficient for HG2, as long as the pore dimensions are large enough, the pore structure is sufficiently open and the loading of HG2 is not too high. Under such circumstances, cyclooctene is converted into linear polymers, which undergo conversion into the desired cyclic oligomers through backbiting. Reaction rates may be as high as those of the homogeneous reaction and product distributions are identical under the conditions of high contact times. If the above criteria are not fulfilled, diffusional control will govern the reaction rate and the product selectivity, leading to slower reaction rates and mixtures of linear polymers and cyclic oligomers. Only under very high contact times is the thermodynamic product distribution, mainly containing cyclic oligomers, obtained.

The presence of water seems not detrimental to HG2, but its presence in the pores retards the metathesis reaction. Therefore, water removal is advised, prior to HG2 immobilization. Care has to be taken though to keep the silanol density high to ensure firm anchorage of HG2 and to avoid formation of reactive siloxanes, which chemically react with and destroy HG2.

Overall, TUD-1 with its large pores and open structure, loaded with 0.2 wt% Ru (1.2 wt% HG2), was recognized as the most privileged catalyst to perform ROMP of cyclic olefins. With this immobilized catalyst, a TON of 18 000 was reached in a continuous experiment under non-optimized ambient conditions. This catalyst performed also excellently in other metathesis types. In particular, the catalyst appears to have good performance for the conversion of bio-based substrates like methyl oleate and butyl vinyl glycolate, indicating that immobilized metathesis catalysts can play an important role in the conversion of biomass like oils^{112–115} and biomass-derived olefins^{103,104,116} into commodity chemicals like polymer building blocks.⁴

Experimental synthesis and characterization of the support

The following silica materials were synthesized according to the literature: TUD-1,¹¹⁷ MCM-41,⁷⁴ SBA-15 (rope-like morphology),¹¹⁸ SBA-15 (fiber-like morphology),¹¹⁹ MCM-48,¹²⁰ KIT-6,¹²¹ SBA-3,¹²² SBA-16,⁸² KIT-5,⁷⁷ Si-VPI-5,¹²³ silicalite-1,¹²⁴ and AlPO₄-5.¹²⁵ Silica gel 239 (Grace) and Silica gel 60 (Davisil grade, Sigma-Aldrich) were used as-received. Scanning electron microscopy (SEM) images were recorded on a JEOL JSM-6010 JV microscope. Before measurements, the

materials were coated with gold using a JEOL JSC-1300 sputter coater. The crystallinity of the mesoporous materials was verified by small-angle X-ray scattering (SAXS) on a SMART 6000 diffractometer with a Cu source and a 2D CCD detector. Determination of the textural parameters of the support was carried out *via* nitrogen physisorption on a Micromeritics TriStar 3000 surface and porosity analyzer. The pore size was calculated according to non-local density functional theory methods^{126–128} and the pore volumes were determined with the *t*-plot method. Quantification of the silica silanols was carried out *via* FT-IR spectroscopy. Spectra were recorded on a Nicolet 6700 spectrometer, equipped with a DTGS detector and a KBr beam splitter (256 scans, resolution of 2 cm⁻¹). Self-supporting wafers were placed in a vacuum IR-cell and dehydrated under vacuum for 1 h at 50 °C prior to measurements. The dry samples were heated progressively at 5 °C min⁻¹ and kept at each temperature for 45 minutes. All of the samples (except the one dried at 50 °C) were measured at 150 °C. The molar integrated absorption coefficient $\epsilon_{(\nu+\delta)_{\text{OH}}}$ used was 0.16 cm² μmol⁻¹.⁸⁴ Near-infrared diffuse reflectance measurements (NIR DRS) were performed on an Agilent Cary 5000 spectrophotometer. Samples were placed in a quartz tube with a window, and were dried at 50 °C under vacuum (10 mbar) or at 150 °C (under atmospheric pressure) before measurement. ²⁹Si MAS NMR spectra were recorded on a Bruker AMX300 spectrometer (*B*₀ = 7.0 T). At this field, the resonance frequency of ²⁹Si is 59.6 MHz. The samples were packed in a 4 mm zirconia rotor. Tetramethylsilane was used as a chemical shift reference. 2056 scans were accumulated with a recycle delay of 120 s. The spinning frequency of the rotor was 6000 Hz. For determination of the presence of reactive strained siloxanes on MCM-41 and TUD-1, the supports were thermally pretreated under nitrogen atmosphere at 900 °C and 700 °C, respectively. The dried samples were reacted with dichlorodimethylsilane (DCDMS) under nitrogen atmosphere to cover all surface hydroxyls, followed by drying under vacuum. The silanol-deactivated powders were introduced into a U-tube reactor, brought into contact with an NH₃ flow (3 mL s⁻¹) and heated to 500 °C, which was maintained for 6 h to react the powders with strained siloxanes.¹²⁹ To verify the coverage of surface hydroxyls by DCDMS and reaction of siloxanes with NH₃, FT-IR spectra were taken as described above. TGA analyses were conducted on a TGA Q500 (TA Instruments). Determination of the amount of water in the pores was carried out under a flow of dry nitrogen from room temperature to 500 °C at a heating rate of 3 °C min⁻¹.

Immobilization of the support and characterization of the heterogeneous catalyst

Immobilization of the 2nd generation Hoveyda–Grubbs catalyst (HG2) (Sigma-Aldrich, 97%) was performed in an inert nitrogen atmosphere. The precatalyst was dissolved in toluene (Acros Organics, 99.5%) and added to the pre-dried silica source. Typically, a 1.57 mmol L⁻¹ solution of HG2 in toluene (5 mL) was added to 0.2 g of a silica support, resulting in a

loading of 0.2–0.3 wt% Ru. The suspension was stirred at room temperature for 45 minutes, filtered and washed thoroughly with hexane (Chem-lab, 99%). After drying, a green powder was obtained, which was stored at $-20\text{ }^{\circ}\text{C}$ to guarantee stability. Determination of the amount of ruthenium immobilized on the support was performed *via* UV-vis spectroscopy analysis of the toluene solution before and after immobilization using a Shimadzu UV-1650PC spectrophotometer. ICP-AES was performed to measure the amount of ruthenium in the solution and to confirm the amount of ruthenium immobilized on the support. Analyses were conducted on a Jobin Yvon Ultima ICP emission spectrometer with argon plasma. Measurements of the atomic emission spectra of ruthenium were conducted at 240.727 nm. Before measurements, the samples were dissolved in a slightly acidic solution (3% HNO_3 in water). Measurements of the immobilized catalysts after reaction to determine the remaining carbon fraction were performed with TGA under a flow of dry oxygen. The weight loss was monitored from room temperature to $600\text{ }^{\circ}\text{C}$ at a heating rate of $3\text{ }^{\circ}\text{C min}^{-1}$. Determination of the amount of water in the pores was carried out under a flow of dry nitrogen from room temperature to $500\text{ }^{\circ}\text{C}$ at a heating rate of $3\text{ }^{\circ}\text{C min}^{-1}$.

Catalytic reactions

The following substrates were used: *cis*-cyclooctene (Acros Organics, 95%), *cis,cis*-1,5-cyclooctadiene (Sigma-Aldrich, $\geq 99\%$), norbornene (Sigma-Aldrich, 99%), diethyl diallylmalonate (Sigma-Aldrich, 98%), methyl oleate (Sigma-Aldrich, 99%), methyl 10-undecenoate (Merck, $\geq 96\%$), 1,7-octadiene (Alfa Aesar, 97%) and methyl (*D,L*)-2-hydroxy-3-butenate (TCI Chemicals, $>96\%$). For batch reactions, glass reactor vials (10 mL) were charged with the catalyst under an atmosphere of nitrogen (except for the catalyst with a non-thermally pretreated support, *e.g.* MCM-41 at $25\text{ }^{\circ}\text{C}$). Stirring tests with increasing amounts of catalysts pointed out that ideal stirring is only achieved when 50 mg or less (Fig. S16[†]) per 5 mL of solvent is used. With higher amounts, the contact time needed to reach the same conversion increases due to insufficient stirring. Therefore, standard reactions were performed with 50 mg of the catalyst. The substrate was dissolved in hexane (5 mL) and added into the glass reactor. The mixture was stirred at $35\text{ }^{\circ}\text{C}$, unless mentioned otherwise. *n*-Undecane (Acros Organics, 99%) was added as an internal standard whenever required. Ethyl vinyl ether (Sigma-Aldrich, 99%) was used as a terminating agent prior to filtration/centrifugation of the heterogeneous catalyst when taking samples. For cross-metathesis and ring-closing metathesis reactions of terminal olefins, an additional balloon filled with argon was used to dilute the ethylene formed during the reaction when hexane was used as a solvent, while for high-boiling compounds, the reaction was performed in hexane under reduced pressure (700 mbar) to remove ethylene. To verify the heterogeneity of the catalyst, a split-test was carried out. After 15 minutes, 2 samples were taken from the

reaction mixture. One was quenched with potassium 2-isocynoacetate (Sigma-Aldrich, 85%) in methanol to quickly deactivate the catalyst, while the other sample was filtered with a $0.45\text{ }\mu\text{m}$ PTFE filter to retain the immobilized catalyst and was further stirred at the same reaction temperature. The conversion of the filtered sample was compared to that of the quenched sample at the end of the reaction. For continuous reactions, a glass reactor was charged with the catalyst (110 mg of HG2/TUD-1, 0.20 wt% Ru; mixed with unloaded pellets of TUD-1) and kept in place using quartz wool and glass beads. Cyclooctene (0.4 mol L^{-1}) was pumped at a rate of 80 mL h^{-1} over the catalyst bed at room temperature.

Analysis. GC analysis of the volatile products was carried out on an Agilent 6890 GC equipped with a flame ionization detector (FID), in which the products were separated over an HP-5 capillary column. Identification of the reaction products, separated over an HP-5 column, was carried out *via* GC-MS on an Agilent 6890N GC with an Agilent 5973N mass selective detector. GPC analysis was performed for the separation of bigger oligomers using a Waters e2695 Separations Module and a Waters 2414 RI detector. The stationary phase consists of a Varian M-Gel 3 mixed column. A 1 mL min^{-1} flow of THF was used. Polystyrene standards were used for calibration. Molecular weight determined fractions: cyclic oligomers, *i.e.* C16–C56 oligomers of cyclooctene ($M_w = 220\text{--}770\text{ g mol}^{-1}$) or $>\text{C}56$ if mentioned; linear oligomers, *i.e.* short linear fragments of cyclooctene ($M_w = 200\text{--}3000\text{ g mol}^{-1}$); linear polymers ($M_w > 3000\text{ g mol}^{-1}$). $^1\text{H-NMR}$ spectra were recorded on a Bruker Avance 300 MHz spectrometer using DMSO as a solvent.

Acknowledgements

A. D. and B. S. thank FWO-Flanders for its financial support (Project G.0229.12). The authors are grateful to Johan Martens for general financial support through Methusalem. The authors thank Kristof Houthoofd for NMR measurements and interpretation of the data, Iris Cuppens for ICP-AES, Stef Kerkhofs and Gert Brabants for the SAXS measurements and Walter Vermandel for his help with the continuous experiments. The authors also thank Ivo Stassen for the NLDFT calculations.

Notes and references

- 1 K. C. Nicolaou, P. G. Bulger and D. Sarlah, *Angew. Chem., Int. Ed.*, 2005, **44**, 4490–4527.
- 2 R. H. Grubbs, *Tetrahedron*, 2004, **60**, 7117–7140.
- 3 R. H. Grubbs and S. Chang, *Tetrahedron*, 1998, **54**, 4413–4450.
- 4 M. Dusselier, P. Van Wouwe, S. De Smet, R. De Clercq, L. Verbelen, P. Van Puyvelde, F. E. Du Prez and B. F. Sels, *ACS Catal.*, 2013, **3**, 1786–1800.
- 5 C. Samojłowicz, M. Bieniek and K. Grela, *Chem. Rev.*, 2009, **109**, 3708–3742.

- 6 P. Schwab, R. H. Grubbs and J. W. Ziller, *J. Am. Chem. Soc.*, 1996, **118**, 100–110.
- 7 J. C. Mol, *J. Mol. Catal. A: Chem.*, 2004, **213**, 39–45.
- 8 H. Clavier, K. Grela, A. Kirschning, M. Mauduit and S. P. Nolan, *Angew. Chem., Int. Ed.*, 2007, **46**, 6786–6801.
- 9 H. D. Maynard and R. H. Grubbs, *Tetrahedron Lett.*, 1999, **40**, 4137–4140.
- 10 G. C. Vougioukalakis, *Chem. – Eur. J.*, 2012, **18**, 8868–8880.
- 11 M. S. Sanford, J. A. Love and R. H. Grubbs, *J. Am. Chem. Soc.*, 2001, **123**, 6543–6554.
- 12 M. Ulman and R. H. Grubbs, *J. Org. Chem.*, 1999, **64**, 7202–7207.
- 13 J. C. Conrad and D. E. Fogg, *Curr. Org. Chem.*, 2006, **10**, 185–202.
- 14 R. Buffon, A. Choplin, M. Leconte, J. M. Basset, R. Touroude and W. A. Herrmann, *J. Mol. Catal.*, 1992, **72**, L7–L10.
- 15 M. Chabanas, A. Baudouin, C. Copéret and J.-M. Basset, *J. Am. Chem. Soc.*, 2001, **123**, 2062–2063.
- 16 R. P. Saint-Arroman, M. Chabanas, A. Baudouin, C. Copéret, J.-M. Basset, A. Lesage and L. Emsley, *J. Am. Chem. Soc.*, 2001, **123**, 3820–3821.
- 17 M. P. Conley, W. P. Forrest, V. Mougél, C. Copéret and R. R. Schrock, *Angew. Chem.*, 2014, **126**, 14445–14448.
- 18 V. Mougél, C. B. Santiago, P. A. Zhizhko, E. N. Bess, J. Varga, G. Frater, M. S. Sigman and C. Copéret, *J. Am. Chem. Soc.*, 2015, **137**, 6699–6704.
- 19 T. S. Halbach, S. Mix, D. Fischer, S. Maechling, J. O. Krause, C. Sievers, S. Blechert, O. Nuyken and M. R. Buchmeiser, *J. Org. Chem.*, 2004, **70**, 4687–4694.
- 20 J. O. Krause, S. H. Lubbad, O. Nuyken and M. R. Buchmeiser, *Macromol. Rapid Commun.*, 2003, **24**, 875–878.
- 21 J. O. Krause, O. Nuyken, K. Wurst and M. R. Buchmeiser, *Chem. – Eur. J.*, 2004, **10**, 777–784.
- 22 D. Bek, N. Žilková, J. Dědeček, J. Sedláček and H. Balcar, *Top. Catal.*, 2009, **53**, 200–209.
- 23 P. Nieczypor, W. Buchowicz, W. J. N. Meester, F. P. J. T. Rutjes and J. C. Mol, *Tetrahedron Lett.*, 2001, **42**, 7103–7105.
- 24 K. Vehlow, S. Maechling, K. Köhler and S. Blechert, *J. Organomet. Chem.*, 2006, **691**, 5267–5277.
- 25 L. Yang, M. Mayr, K. Wurst and M. R. Buchmeiser, *Chem. – Eur. J.*, 2004, **10**, 5761–5770.
- 26 D. Bek, H. Balcar, N. Žilková, A. T. Zúkal, M. Horáček and J. I. Čejka, *ACS Catal.*, 2011, **1**, 709–718.
- 27 L. Li and J.-L. Shi, *Adv. Synth. Catal.*, 2005, **347**, 1745–1749.
- 28 S. Randl, N. Buschmann, S. J. Connon and S. Blechert, *Synlett*, 2001, **10**, 1547–1550.
- 29 M. Mayr, B. Mayr and M. R. Buchmeiser, *Angew. Chem., Int. Ed.*, 2001, **40**, 3839–3842.
- 30 J. P. Gallivan, J. P. Jordan and R. H. Grubbs, *Tetrahedron Lett.*, 2005, **46**, 2577–2580.
- 31 K. Melis, D. E. De Vos, P. A. Jacobs and F. Verpoort, *J. Mol. Catal. A: Chem.*, 2001, **169**, 47–56.
- 32 K. H. Park, S. Kim and Y. K. Chung, *Bull. Korean Chem. Soc.*, 2008, **29**, 2057–2060.
- 33 A. Monge-Marcet, R. Pleixats, X. Cattoën and M. Wong Chi Man, *J. Mol. Catal. A: Chem.*, 2012, **357**, 59–66.
- 34 S. T. Nguyen and R. H. Grubbs, *J. Organomet. Chem.*, 1995, **497**, 195–200.
- 35 S. C. Schürer, S. Gessler, N. Buschmann and S. Blechert, *Angew. Chem., Int. Ed.*, 2000, **39**, 3898–3901.
- 36 I. Karamé, M. Boualleg, J.-M. Camus, T. K. Maishal, J. Alauzun, J.-M. Basset, C. Copéret, R. J. P. Corriu, E. Jeanneau, A. Mehdi, C. Reyé, L. Veyre and C. Thieuleux, *Chem. – Eur. J.*, 2009, **15**, 11820–11823.
- 37 A. G. M. Barrett, S. M. R. Cramp and S. Richard, *Org. Lett.*, 1999, **1**, 1083–1086.
- 38 G. Borja, R. Pleixats, R. Alibés, X. Cattoën and M. W. C. Man, *Molecules*, 2010, **15**, 5756–5767.
- 39 X. Elias, R. Pleixats, M. W. C. Man and J. J. E. Moreau, *Adv. Synth. Catal.*, 2007, **349**, 1701–1713.
- 40 D. Fischer and S. Blechert, *Adv. Synth. Catal.*, 2005, **347**, 1329–1332.
- 41 S. B. Garber, J. S. Kingsbury, B. L. Gray and A. H. Hoveyda, *J. Am. Chem. Soc.*, 2000, **122**, 8168–8179.
- 42 A. Keraani, C. Fischmeister, T. Renouard, M. Le Floch, A. Baudry, C. Bruneau and M. Rabiller-Baudry, *J. Mol. Catal. A: Chem.*, 2012, **357**, 73–80.
- 43 J. S. Kingsbury, S. B. Garber, J. M. Giftos, B. L. Gray, M. M. Okamoto, R. A. Farrer, J. T. Fourkas and A. H. Hoveyda, *Angew. Chem., Int. Ed.*, 2001, **40**, 4251–4256.
- 44 J. Lim, S. S. Lee, S. N. Riduan and J. Y. Ying, *Adv. Synth. Catal.*, 2007, **349**, 1066–1076.
- 45 J. Lim, S. Seong Lee and J. Y. Ying, *Chem. Commun.*, 2010, **46**, 806.
- 46 S. Varray, R. Lazaro, J. Martinez and F. Lamaty, *Organometallics*, 2003, **22**, 2426–2435.
- 47 Q. Yao, *Angew. Chem., Int. Ed.*, 2000, **39**, 3896–3898.
- 48 H. Zhang, Y. Li, S. Shao, H. Wu and P. Wu, *J. Mol. Catal. A: Chem.*, 2013, **372**, 35–43.
- 49 Q. T. Easter, V. Trauschke and S. A. Blum, *ACS Catal.*, 2015, **5**, 2290–2295.
- 50 H. Staub, F. Kleitz and F.-G. Fontaine, *Microporous Mesoporous Mater.*, 2013, **175**, 170–177.
- 51 H. Yang, Z. Ma, T. Zhou, W. Zhang, J. Chao and Y. Qin, *ChemCatChem*, 2013, **5**, 2278–2287.
- 52 Q. Li, T. Zhou and H. Yang, *ACS Catal.*, 2015, **5**, 2225–2231.
- 53 C. Copéret and J. M. Basset, *Adv. Synth. Catal.*, 2007, **349**, 78–92.
- 54 H. Balcar and J. Čejka, *Coord. Chem. Rev.*, 2013, **257**, 3107–3124.
- 55 H. Balcar and J. Čejka, *Macromol. Symp.*, 2010, **293**, 43–47.
- 56 M. P. Conley, C. Copéret and C. Thieuleux, *ACS Catal.*, 2014, **4**, 1458–1469.
- 57 F. B. Hamad, C. Kai, Y. Cai, Y. Xie, Y. Lu, F. Ding, Y. Sun and F. Verpoort, *Curr. Org. Chem.*, 2013, **17**, 2592–2608.
- 58 B. van Berlo, K. Houthoofd, B. F. Sels and P. A. Jacobs, *Adv. Synth. Catal.*, 2008, **350**, 1949–1953.
- 59 J. Cabrera, R. Padilla, M. Bru, R. Lindner, T. Kageyama, K. Wilckens, S. L. Balof, H.-J. Schanz, R. Dehn, J. H. Teles, S.

- Deuerlein, K. Müller, F. Rominger and M. Limbach, *Chem. – Eur. J.*, 2012, **18**, 14717–14724.
- 60 M. Bru, R. Dehn, J. H. Teles, S. Deuerlein, M. Danz, I. B. Müller and M. Limbach, *Chem. – Eur. J.*, 2013, **19**, 11661–11671.
- 61 W. Solodenko, A. Doppiu, R. Frankfurter, C. Vogt and A. Kirschning, *Aust. J. Chem.*, 2013, **66**, 183.
- 62 H. Balcar, T. Shinde, N. Žilková and Z. Bastl, *Beilstein J. Org. Chem.*, 2011, **7**, 22–28.
- 63 H. Yang, Z. Ma, Y. Wang, Y. Wang and L. Fang, *Chem. Commun.*, 2010, **46**, 8659.
- 64 T. Shinde, N. Žilková, V. Hanková and H. Balcar, *Catal. Today*, 2012, **179**, 123–129.
- 65 J. Pastva, K. Skowerski, S. J. Czarnocki, N. Žilková, J. Čejka, Z. Bastl and H. Balcar, *ACS Catal.*, 2014, **4**, 3227–3236.
- 66 R. L. Dehn, S. Deuerlein, M. Danz, M. Limbach and J. H. Teles, *US Pat.*, US20120165588, 2012.
- 67 Z. Jia and M. J. Monteiro, *J. Polym. Sci., Part A: Polym. Chem.*, 2012, **50**, 2085–2097.
- 68 H. R. Kricheldorf, *J. Polym. Sci., Part A: Polym. Chem.*, 2010, **48**, 251–284.
- 69 A. M. Gessler, *US Pat.*, US2553651, 1951.
- 70 J. F. Hampton, *US Pat.*, US3465016, 1969.
- 71 C. Sell, Ingredients for the modern perfumery industry, in *The Chemistry of Fragrances: From Perfumer to Consumer*, ed. C. S. Sell, The Royal Society of Chemistry, Cambridge, 2006, pp. 95–106.
- 72 M. K. Samantaray, J. Alauzun, D. Gajan, S. Kavitate, A. Mehdi, L. Veyre, M. Lelli, A. Lesage, L. Emsley, C. Copéret and C. Thieuleux, *J. Am. Chem. Soc.*, 2013, **135**, 3193–3199.
- 73 Information about impurities silica gels: Catalog Resins & Media p. 5, Sigma-Aldrich.
- 74 B. Pauwels, G. Van Tendeloo, C. Thoelen, W. Van Rhijn and P. Jacobs, *Adv. Mater.*, 2001, **13**, 1317–1320.
- 75 H. Zhang, J. Sun, D. Ma, X. Bao, A. Klein-Hoffmann, G. Weinberg, D. Su and R. Schlögl, *J. Am. Chem. Soc.*, 2004, **126**, 7440–7441.
- 76 S. Polarz, B. Völker and F. Jeremias, *Dalton Trans.*, 2010, **39**, 577–584.
- 77 F. Kleitz, D. Liu, G. M. Anilkumar, I.-S. Park, L. A. Solovyov, A. N. Shmakov and R. Ryoo, *J. Phys. Chem. B*, 2003, **107**, 14296–14300.
- 78 H.-J. Kim, K.-S. Jang, P. Galebach, C. Gilbert, G. Tompsett, W. C. Conner, C. W. Jones and S. Nair, *J. Membr. Sci.*, 2013, **427**, 293–302.
- 79 Z. Shan, J. C. Jansen, L. Marchese and T. Maschmeyer, *Microporous Mesoporous Mater.*, 2001, **48**, 181–187.
- 80 S. Telalovic, A. Ramanathan, G. Mul and U. Hanefeld, *J. Mater. Chem.*, 2010, **20**, 642–658.
- 81 R. Maheswari, R. Anand and G. Imran, *J. Porous Mater.*, 2012, **19**, 283–288.
- 82 F. Kleitz, T.-W. Kim and R. Ryoo, *Langmuir*, 2006, **22**, 440–445.
- 83 L. T. Zhuravlev, *Colloids Surf., A*, 2000, **173**, 1–38.
- 84 J.-P. Gallas, J.-M. Goupil, A. Vimont, J.-C. Lavalley, B. Gil, J.-P. Gilson and O. Miserque, *Langmuir*, 2009, **25**, 5825–5834.
- 85 A. A. Christy, *Adv. Mater. Res.*, 2013, **650**, 66–71.
- 86 K. Wan, Q. Liu and C. Zhang, *Mater. Lett.*, 2003, **57**, 3839–3842.
- 87 S. Shioji, M. Hanada, Y. Hayashi, K. Tokami and H. Yamamoto, *Adv. Powder Technol.*, 2007, **18**, 467–483.
- 88 P. Der Voort, *J. Chem. Soc., Faraday Trans.*, 1990, **86**, 3747–3750.
- 89 K. Unger, *Porous Silica*, Elsevier Science, 1979.
- 90 D. W. Sindorf and G. E. Maciel, *J. Am. Chem. Soc.*, 1983, **105**, 3767–3776.
- 91 B. Fubini, V. Bolis, A. Cavenago and P. Ugliengo, *J. Chem. Soc., Faraday Trans.*, 1992, **88**, 277–289.
- 92 J. P. Blitz, C. C. Meverden and R. E. Diebel, *Langmuir*, 1998, **14**, 1122–1129.
- 93 B. A. Morrow, I. A. Cody and L. S. M. Lee, *J. Phys. Chem.*, 1976, **80**, 2761–2767.
- 94 H. Staub, R. Guillet-Nicolas, N. Even, L. Kayser, F. Kleitz and F.-G. Fontaine, *Chem. – Eur. J.*, 2011, **17**, 4254–4265.
- 95 M. Ide, M. El-Roz, E. De Canck, A. Vicente, T. Planckaert, T. Bogaerts, I. Van Driessche, F. Lynen, V. Van Speybroeck, F. Thybault-Starzyk and P. van der Voort, *Phys. Chem. Chem. Phys.*, 2013, **15**, 642.
- 96 J. D. Robert, in *Catalysis for the Conversion of Biomass and Its Derivatives*, ed. M. Behrens and A. K. Datye, The Max Planck Research Library for the History and Development of Knowledge, Berlin, 2013, pp. 255–286.
- 97 D. Luss, *Diffusion-reaction Interactions in Catalyst Pellets*, Taylor & Francis, Texas, 1986.
- 98 S. Monfette and D. E. Fogg, *Chem. Rev.*, 2009, **109**, 3783–3816.
- 99 H. Höcker, W. Reimann, L. Reif and K. Riebel, *J. Mol. Catal.*, 1980, **8**, 191–202.
- 100 L. Reif and H. Hoecker, *Macromolecules*, 1984, **17**, 952–956.
- 101 H. Jacobson and W. H. Stockmayer, *J. Chem. Phys.*, 1950, **18**, 1600–1606.
- 102 Z. R. Chen, J. P. Claverie, R. H. Grubbs and J. A. Kornfield, *Macromolecules*, 1995, **28**, 2147–2154.
- 103 A. Blencowe and G. G. Qiao, *J. Am. Chem. Soc.*, 2013, **135**, 5717–5725.
- 104 S. Kavitate, M. K. Samantaray, R. Dehn, S. Deuerlein, M. Limbach, J. A. Schachner, E. Jeanneau, C. Copéret and C. Thieuleux, *Dalton Trans.*, 2011, **40**, 12443.
- 105 S. M. Rountree, M. C. Lagunas, C. Hardacre and P. N. Davey, *Appl. Catal., A*, 2011, **408**, 54–62.
- 106 B. Van Berlo, J. Dijkmans, K. Houthoofd, M. Tromp, I. Hermans, P. Jacobs and B. F. Sels, *Detroit*, U.S.A., 2011.
- 107 R. Klaewkla, M. Arend and W. F. Hoelderich, in *Mass Transfer – Advanced Aspects*, ed. H. Nakajima, 2011.
- 108 H. Höcker, W. Reimann, K. Riebel and Z. Szentivanyi, *Macromol. Chem. Phys.*, 1976, **177**, 1707–1715.
- 109 E. Thorn-Csányi and K. Ruhland, *Macromol. Chem. Phys.*, 1999, **200**, 1662–1671.
- 110 C. W. Bielawski and R. H. Grubbs, *Prog. Polym. Sci.*, 2007, **32**, 1–29.
- 111 A. K. Chatterjee, T.-L. Choi, D. P. Sanders and R. H. Grubbs, *J. Am. Chem. Soc.*, 2003, **125**, 11360–11370.

- 112 A. Nickel, T. Ung, G. Mkrtumyan, J. Uy, C. Lee, D. Stoianova, J. Papazian, W.-H. Wei, A. Mallari, Y. Schrodi and R. Pederson, *Top. Catal.*, 2012, 55, 518–523.
- 113 J. C. Mol and R. Buffon, *J. Braz. Chem. Soc.*, 1998, 9, 1–11.
- 114 J. C. Mol, *Green Chem.*, 2002, 4, 5–13.
- 115 R. Kadyrov, C. Azap, S. Weidlich and D. Wolf, *Top. Catal.*, 2012, 55, 538–542.
- 116 Y. Yang, X. Wei, F. Zeng and L. Deng, *Green Chem.*, 2015, DOI: 10.1039/C5GC01922B.
- 117 J. C. Jansen, Z. Shan, T. Maschmeyer, L. Marchese, W. Zhou and N. V. D. Puil, *Chem. Commun.*, 2001, 713–714.
- 118 K. Flodström and V. Alfredsson, *Microporous Mesoporous Mater.*, 2003, 59, 167–176.
- 119 D. Zhao, *Science*, 1998, 279, 548–552.
- 120 K. Schumacher, M. Grün and K. K. Unger, *Microporous Mesoporous Mater.*, 1999, 27, 201–206.
- 121 A. Vinu, N. Gokulakrishnan, V. V. Balasubramanian, S. Alam, M. P. Kapoor, K. Ariga and T. Mori, *Chem. – Eur. J.*, 2008, 14, 11529–11538.
- 122 O. A. Anunziata, A. R. Beltramone, M. L. Martínez and L. L. Belon, *J. Colloid Interface Sci.*, 2007, 315, 184–190.
- 123 S. del Val, T. Blasco, E. Sastre and J. Perez-Pariente, *J. Chem. Soc., Chem. Commun.*, 1995, 731–732.
- 124 C. Shao, X. Li, S. Qiu, F.-S. Xiao and O. Terasaki, *Microporous Mesoporous Mater.*, 2000, 39, 117–123.
- 125 M. Fang, H. Du, W. Xu, X. Meng and W. Pang, *Microporous Mater.*, 1997, 9, 59–61.
- 126 P. I. Ravikovitch, G. L. Haller and A. V. Neimark, *Adv. Colloid Interface Sci.*, 1998, 76–77, 203–226.
- 127 M. Jaroniec, M. Kruk, J. P. Olivier and S. Koch, in *Stud. Surf. Sci. Catal.*, ed. G. K. K. Unger and J. P. Baselt, Elsevier, 2000, vol. 128, pp. 71–80.
- 128 J. Landers, G. Y. Gor and A. V. Neimark, *Colloids Surf., A*, 2013, 437, 3–32.
- 129 T. Asefa, M. Kruk, N. Coombs, H. Grondey, M. J. MacLachlan, M. Jaroniec and G. A. Ozin, *J. Am. Chem. Soc.*, 2003, 125, 11662–11673.
- 130 M. S. Holm, Y. J. Pagan-Torres, S. Saravanamurugan, A. Riisager, J. A. Dumesic and E. Taarning, *Green Chem.*, 2012, 14, 702–706.
- 131 M. Dusselier, P. Van Wouwe, F. de Clippel, J. Dijkmans, D. W. Gammon and B. F. Sels, *ChemCatChem*, 2013, 5, 569–575.